Master Thesis in Geographical Information Science nr 175

Estimating lake water volume fluctuations using Sentinel-2 and ICESat-2 remote sensing data

Pavlos Alexantonakis

2024

Department of

Physical Geography and Ecosystems Science

Lund University

Sweden

Estimating lake water volume fluctuations using Sentinel-2 and ICESat-2 remote sensing data

Pavlos Alexantonakis

Master thesis, 30 credits, in Geographical Information Systems

Supervisor

Prof. David Tenenbaum

Department of Physical Geography and Ecosystem Science

Lund University, Sweden

Abstract

This study focuses on the estimation of lake water volume fluctuations using open-source remote sensing data and evaluates its accuracy. The research follows a three-step methodology, starting with water area estimation from Sentinel-2 imagery, followed by water level estimation using ICESat-2 satellite data, and concluding with the calculation of lake water volume differences, testing the regression modeling and Triangular Irregular Networks (TINs).

For the water extent estimation, three different methods are being compared – Normalized Difference Water Index (NDWI), Modified Normalized Difference Water Index (MNDWI), and Random Forest machine learning algorithm - against manual digitization. All three methods yield accurate results on the quantitative comparison, with performance metrics consistently exceeding 0.95, indicating the absence of a clear preference among these approaches. During the qualitative comparison, misclassified areas were revealed, indicating the problems caused by clouds, shadows and leaves upon the lake which sometime makes the process of accurately map the water extent difficult even for the human eye.

For the water level estimation, ICESat-2 satellite observations were found to be accurate in lake water level monitoring, with a standard deviation of approximately 5 cm, surpassing the nominal accuracy of 6.1 cm. However, limitations are noted in terms of temporal resolution, impacting their use in combination with Sentinel-2 acquisitions.

Finally, for the estimation of water volume fluctuations, the research explores two distinct approaches for calculating water volumes within open water surfaces. The first approach employs regression modeling, deriving a regression equation to estimate water volumes based on area computations. The second approach involves Triangular Irregular Networks (TINs). However, the research discerns that the latter method is not applicable in cases where a significant difference in scale between vertical and horizontal changes exists.

In conclusion, the presented methodology can potentially have benefits for decision-makers and water organizations since it utilizing open-source data and tools for the estimation of lake water volumes. Future work may explore more sophisticated data-driven approaches, including convolutional neural networks, and the incorporation of additional data sources, such as altimetric data from platforms like Jason-2, to improve accuracy and address limitations related to clouds and temporal resolution.

Content

List of Tables

List of Figures

Chapter 1 - Introduction

1.1 Overview

Lake water is essential for many human activities, including water provisioning, fisheries, flood attenuation, and recreational purposes. Lake water also plays an important role in global biogeochemical cycles, and in water, carbon, and nutrient balances. Overexploitation of freshwater resources threatens the capacity of ecosystems to fulfill their vital roles in the future (Fluet-Chouinard et al., 2017) and can also cause ground subsidence, which can be hazardous to anthropogenic environments. Since all domestic, industrial, irrigation, hydropower sectors make extensive use of inland water, it is important to have accurate knowledge of the availability of these water resources, to better protect and manage them and to understand the climate change impacts of their use (Busker et al., 2019).

The volume of water stored in lakes and reservoirs can vary seasonally with the balance being affected by various input and output factors. Input is dependent on precipitation and river inflow, and is also correlated with discharge from communities and industries, seepage, groundwater etc. On the outflow level, events and processes such as evaporation, groundwater percolation, withdrawals, and river outflow greatly affect these volumes (Duan & Bastiaanssen, 2013).

There are different ways to estimate the volume of lake waters, most of which rely on combining information describing the surface area of the water with bathymetry data describing water body depth. However, both bathymetry and shore topography data are often difficult to acquire, and collecting such information can be a time and resource consuming process (Lu et al., 2013). The low cost and high spatiotemporal resolution of remote sensing data should be examined in order to understand the advantages and limitations of related approaches with respect to the water volume estimation problem. Specifically, water surface level information from altimetry data (ICESat-2) and water surface area from multispectral imagery (Sentinel-2) can be used to estimate lake water volume changes between consecutive dates.

Some research has already been done in this field with Duan & Bastiaanssen (2013), Lu et al., (2013), Bhagwat et al. (2019) and Busker et al. (2019), estimating inland water volume variations. In those studies, area and elevation information has been combined to estimate water volume changes, with the former coming from remote sensing and the latter coming either from ground measurements or existing datasets. The scientific gap that this project will try to address is the feasibility of applying an automated method that will only use open-source remote sensing products for the estimation of water volumes in lakes. This research focus on the lake water volume estimation problem, by exploiting different state of the art techniques. The project consists of three methodological steps. The first step is the extraction of the water area from optical satellite imagery. The second step is the extraction of water level using satellite altimetry data. The third step is the combination of spatial and height information (the outputs of two previous steps) to obtain volumetric information. This is applied to a case study in the Kastoria Lake, Greece.

1.2 Objectives and research questions

The overall objective of this research is to develop a methodology based on openly available remote sensing data for the estimation of lake water volumes, and to evaluate its accuracy. This research will accomplish this via three specific objectives.

1. The first objective is related to the performance of three remote sensing approaches for water spatial extent estimation. Accuracy assessment will be performed on water spatial extent estimations extracted from a) the Normalized Difference Water Index (NDWI), b) the Modified Normalized Difference Water Index (MNDWI) and c) a supervised machine learning algorithm (Random Forest) in respect to water spatial extent extracted by manual digitization of Sentinel-2 satellite imagery.

   Research question:

   - What is the relative degree of performance of the aforementioned remote sensing indices approaches and the supervised machine learning algorithm, as compared to the manual digitization results which are considered as ground truth? Degree of performance is quantified by the following metrics: overall accuracy, precision, recall and F1 score (described in Section 3.1.4).

2. Evaluate the potential use of ICESat-2 satellite observations for lake water level monitoring. Assess the temporal frequency, the spatial density and the accuracy of the lake water level observations.

   Research question:

   - What is the accuracy of lake water level observations (in terms of standard deviations) over the lake of interest and how does it compare to the reported nominal accuracy?

3. Estimate the lake water volume differences using the established methods of Regression analysis (Bhagwat et al., 2019) and GIS-generated TINs (Triangular Irregular Networks) (Lu et al., 2013).

   Research question:

   - What is the degree of agreement (in terms of root mean square error) of the lake water volume results from the aforementioned lake water volume approaches?

Chapter 2 – Study Area, Data and Methods Description

2.1 Study Area

This master thesis project will be presented as a case study at Kastoria Lake (Figure1). Kastoria Lake is officially called Lake Orestiada and is located in the Kastoria Regional Unit in northwestern Greece (40°30'54"N 21°18'00"E). At an altitude of 620 m above sea level , it covers more than 28 km^2, its shoreline is 34 km in length and its mean depth is approximately 9 m (Lakes / Orestiada-Lake, NaturaGraeca, n.d.). It's a very important area ecologically, that accommodates a great number of various species of birds and fish and it has been declared as a Monument of Natural Beauty by the Ministry of Culture. It is also a part of the European environmental protection network "Natura 2000" (PDM, Region of Western Macedonia, retrieved on 08-02-2022). The lake has several inflows from its west side while it also has one main outflow at the Haliacmon river.

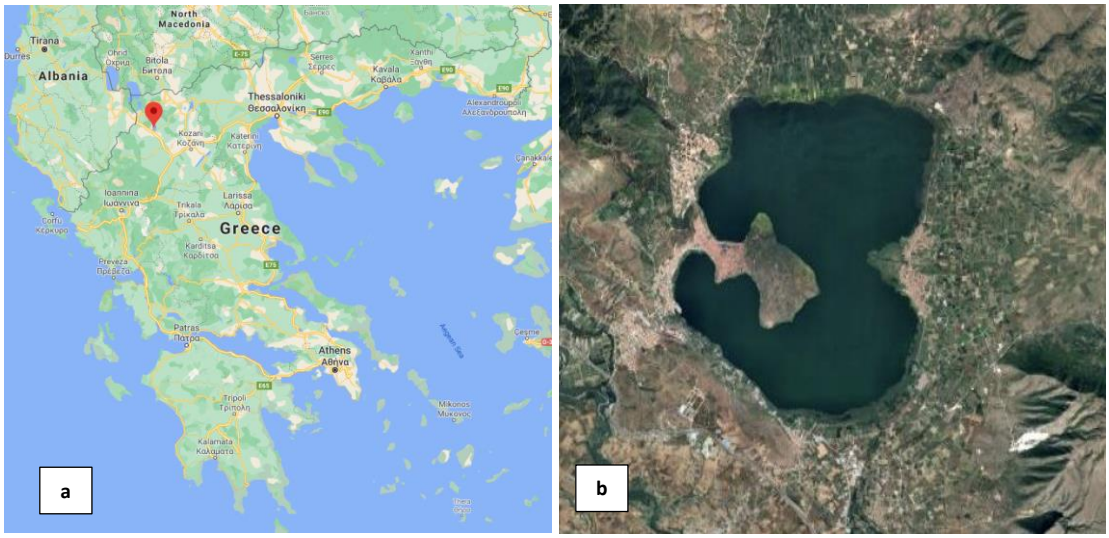

Figure 1: Overview map (a) and satellite image over Lake Kastoria (b). Source: Google imagery 2023©

Besides the importance of the lake for all the aforementioned environmental reasons, it also provides the main water resource for various industrial and agricultural applications in the area.

Other research has taken place due the importance of the lake, mostly concerning the water quality by Matzafleri et al. (2009) and Karamoutsou & Psilovikos (2021), hydrological response to climate change by Voulanas et al (2021) and the hydrogeological conditions of the general area by Gianneli (2009). Yet, no research strictly related to the lake's water volume was found. Additionally, several cases of ground deformation have been reported around the lake and at nearby villages, which can be linked with overexploitation of the water resource and the vast reduction of its volume (Tzampoglou et al., 2023). This is an indication of the importance of this research, and the need for an application for the monitoring of water volume in inland reservoirs.

2.2 Data

The data of interest for this project includes multispectral satellite images from Sentinel-2, and an altimetry dataset from the ICESat-2 LIDAR satellite, both of which are open datasets.

2.2.1 Sentinel-2

The Sentinel-2 data can be downloaded from https://scihub.copernicus.eu. According to the official description at European Space Agency, n.d., accessed on 10/10/2021, Sentinel-2 has 13 spectral bands, four of which have a 10m spatial resolution, six at 20m and the remaining three bands at 60m (Figures 2, 3 and 4). The temporal resolution is defined by the revisit frequency of the satellite to a specific location, which is 5 days. The images are released publicly from ESA under the Creative Commons Attribution 4.0 International license. Sentinel's-2 products are a compilation of 100x100km^2 granules using the UTM/WGS84 coordinate system.

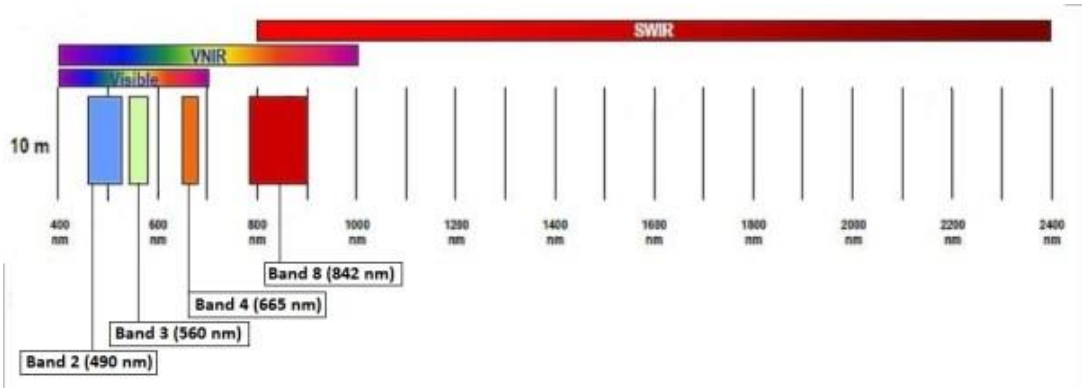

Figure 2: Sentinel-2 10m spatial resolution bands: B2 (490 nm), B3 (560 nm), B4 (665 nm) and B8 (842 nm) source: European Space Agency, n.d., accessed on 10/10/2021.

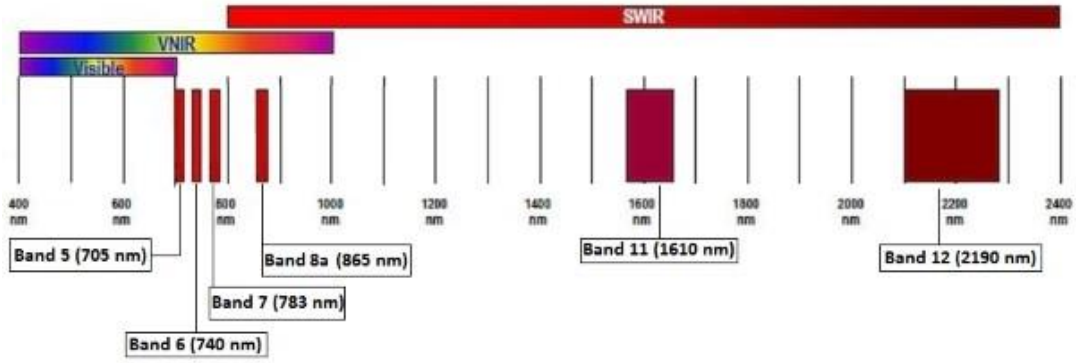

Figure 3: Sentinel-2 20m spatial resolution bands: B5 (705 nm), B6 (740 nm), B7 (783 nm), B8a (865 nm), B11 (1610 nm) and B12 (2190 nm) source: European Space Agency, n.d., accessed on 10/10/2021.

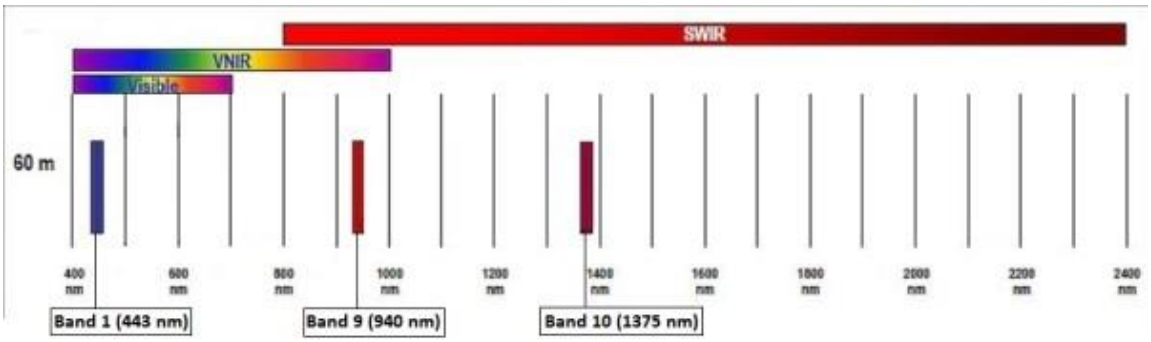

Figure 4: Sentinel-2 60m spatial resolution bands: B1 (443 nm), B9 (940 nm) and B10 (1375 nm) source: European Space Agency, n.d., accessed on 10/10/2021.

A visual inspection was performed to Sentinel-2 data for the time period Nov/2018-Feb/2022, to select all images with a clearly visible shoreline, so that they could be manually digitized. This resulted in a total of 30 images that have been used for the water area estimation process.

2.2.2 ICESat-2

The ICESat-2 LIDAR data are available at National Snow and Ice Data Center (n.d.), with the data product of interest being ATL13, which concerns observations along the satellite's orbital track focusing on surface water features products for inland water bodies. According to the official description, water surface heights are provided as both height above the WGS 84 ellipsoid (ITRF2014 Reference Frame) and height above the Earth Gravitational Model 2008 (EGM2008) mean sea level (MSL). Concerning its accuracy, as the user's guide mentions:

> "… data quality in this product depends largely on the precision of the georeferenced photons input from ATL03 and associated products evaluated prior to use by the ATL13 algorithm. The overall ensemble error per 100 inland water photons is estimated to be 6.1 cm".

The satellite is equipped with a photon-counting laser altimeter called ATLAS, that captures the time it takes for individual photons to travel to the Earth's surface and back. The instrument utilizes 3 pairs of laser beams (6 in total), transmitting 10,000 laser light pulses per second that collect observations in the along-track direction. The beams are organized into a 3x2 array pattern with 3 left and 3 right ones '1r', '2r', '3r', '1l', '2l', '3l', while each pair contains a weak and a strong beam (Figure 5). Those beams of green laser pulses are emitted and received back by the ATLAS instrument, where they are counted by the photon-counting detector. This information is utilized to reconstruct the surface height along the satellite's trajectory, with the temporal resolution of the data product being 91 days (Smith et al., 2019).

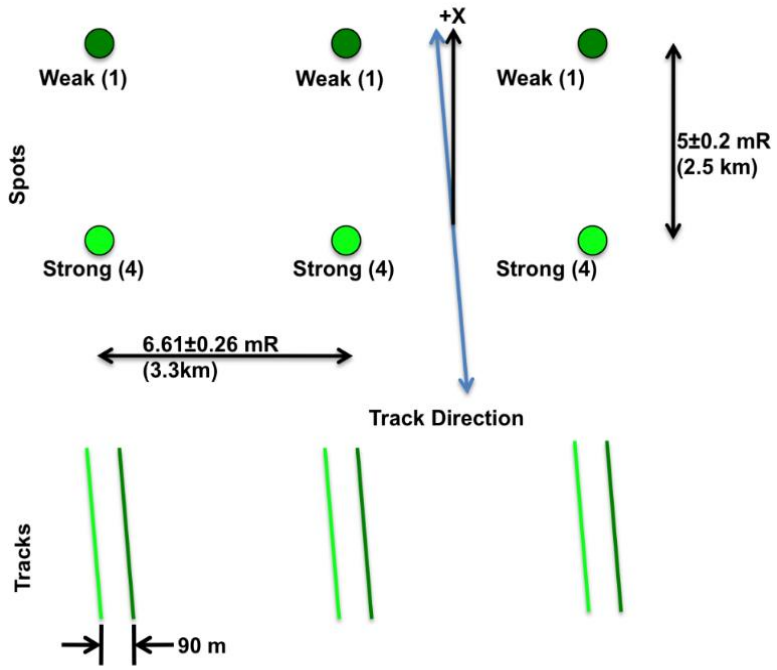

Figure 5: The 6 beams of ICESat-2 (NASA Goddard Space Flight Center, n.d. Accessed on 10/10/2021).

The datasets of Sentinel-2 and ICESat-2 have to be collected at similar dates so that the information can be correlated. Thus, out of all the available dates of each dataset, only the common ones will be kept, since the water extent and water level information have to be combined to estimate the water volume variations.

The common dates where both an ICESat-2 dataset with information in the lake's bounding box, and a Sentinel-2 image with low cloud coverage, were found on 8 occasions, specifically 2019-05-18, 2019-09-14, 2019-11-15, 2019-08-15, 2020-02-12, 2020-08-14, 2021-08-12 and 2022-02-10. Data from these dates were used for the water volume changes estimation.

2.3 Methodological flowchart

The methods for this research project were organized into three stages: water surface area estimation, water altimetry estimation, and finally water volume estimation of the inland reservoir (Figure 6).

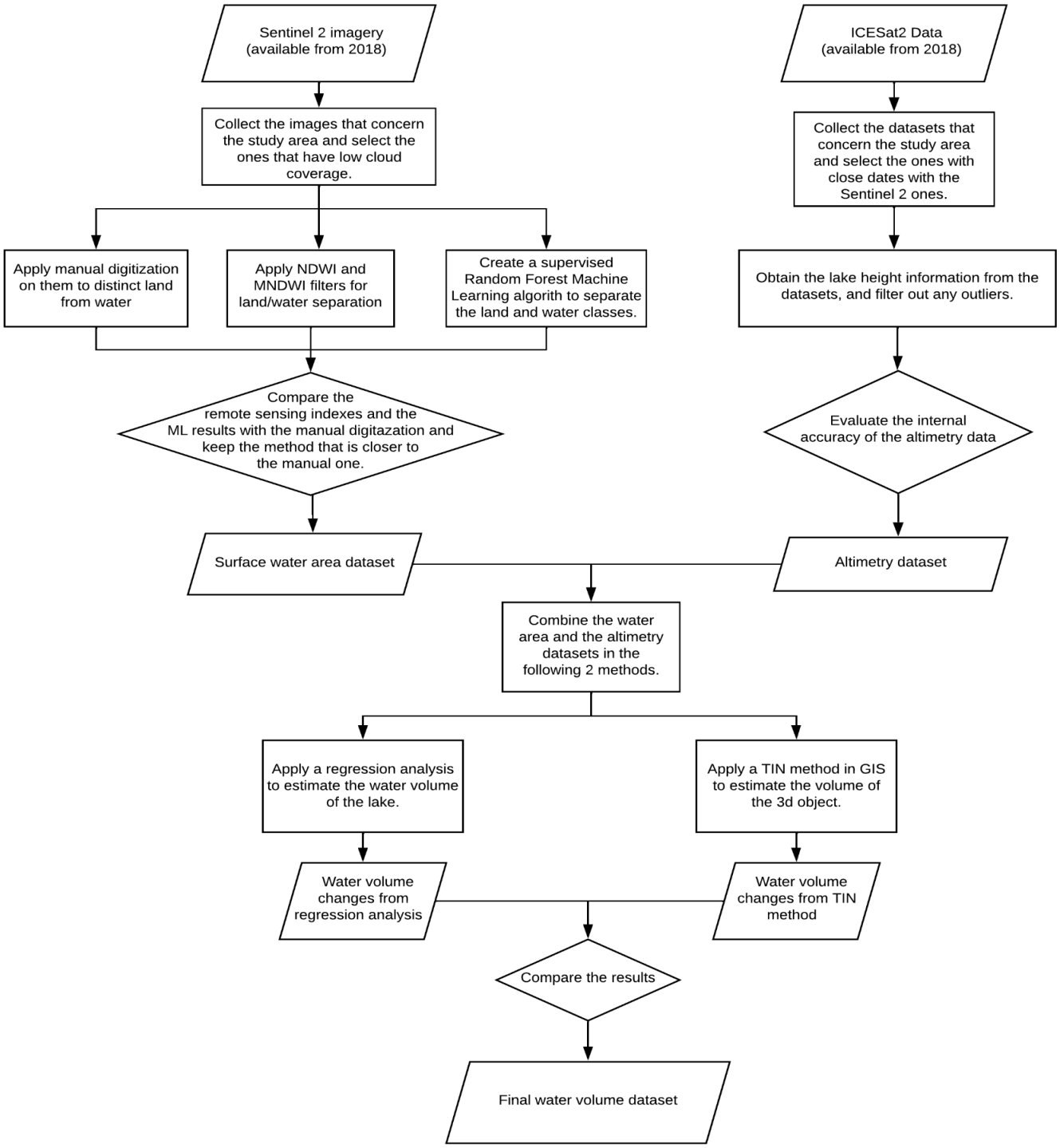

Figure 6: Methodological Flowchart

2.4. Methods Description

2.4.1 Surface water area estimation

For the surface water estimation, three methods that concern water detection have been applied to the satellite images. Those are NDWI and MNDWI thresholding and a Random Forest machine learning algorithm. A manual digitization of the extent of the lake was done on all of the 30 available Sentinel-2 images with acceptably low cloud coverage for the shoreline to be clearly visible. This dataset acted as ground truth for the evaluation of 3 automated methods of water detection. The methodology will be thoroughly explained in this chapter and the analytical code is also attached in the Appendix.

- **NDWI – MNDWI thresholding**

Two remote sensing indexes, the NDWI and the Modified MNDWI were used, in conjunction with a two-class Random Forest machine learning algorithm, trained to distinguish water and non-water pixels. The band equation, when it comes to water bodies detection for $NDWI$ is:

$$NDWI = \frac{Green - NIR}{Green + NIR}$$

while for $MNDWI$ is:

$$MNDWI = \frac{Green - SWIR}{Green + SWIR}$$

with NIR representing the Near Infrared and SWIR the Short-Wave Infrared bands. These indices have been commonly used for water detection purposes (Gabila Buma et al., n.d., Herndon et al., 2020). It is important to state that the spatial resolution of the calculated $NDWI$ and $MNDWI$ indices is 10m. In particular, $Green$ (Band 3 in Figure 2) and NIR (Band 8 in Figure 2) bands are provided at 10m. However, $SWIR$ (Band 11 in Figure 3) is provided at 20m, and a nearest neighbor interpolation was performed to upscale the $SWIR$ to 10 m. This is considered a common preprocessing practice for upscaling satellite multispectral imagery (Hemalatha, 2021).

Firstly, the Sentinel-2 images were imported in QGIS for a visual inspection (Figure 7) and then they were loaded in a python function as arrays, with 2 functions being created for computing NDWI and MNDWI indices per image. Otsu's Thresholding was applied for both indices, classifying each pixel of the images into water/no-water classes (Figure 8). Otsu's Thresholding is a well-known and effective method for selecting a global threshold. The method has been extensively used for surface water mapping due to its simplicity and efficiency in maximizing the inter-class variance while minimizing the weighted within-class variance (Du et al., 2016). It assumes that an image has two classes, which can be separated using an optimal threshold obtained through a gray-level histogram of the image (Otsu, 1979). The two dedicated functions that were developed to process Sentinel-2 images within a Python environment were used to

read the input image as an array and compute pixel-wise NDWI and MNDWI values using the above specified equations.

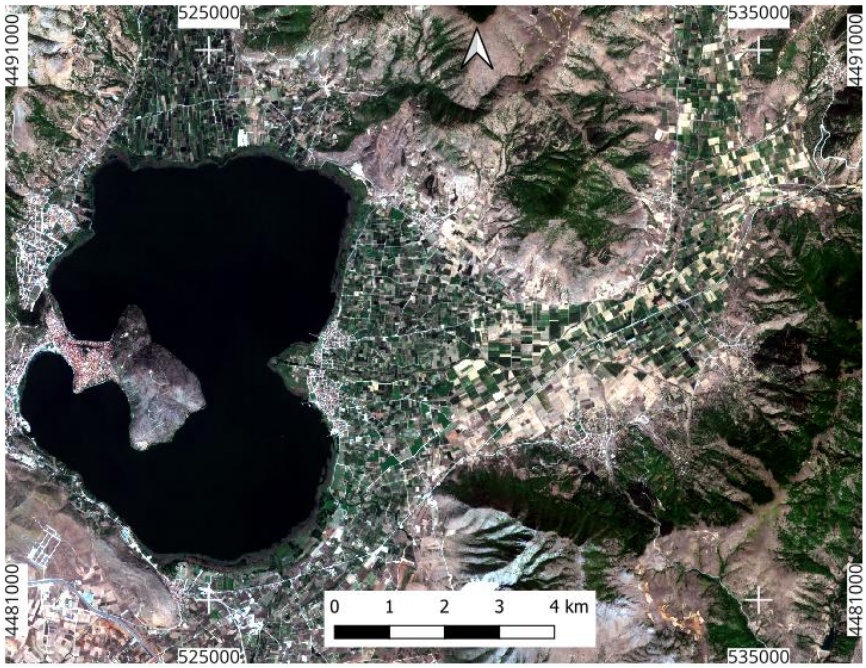

Figure 7: Example of Sentinel 2 image of the Area of Interest. Date: 16-08-2019

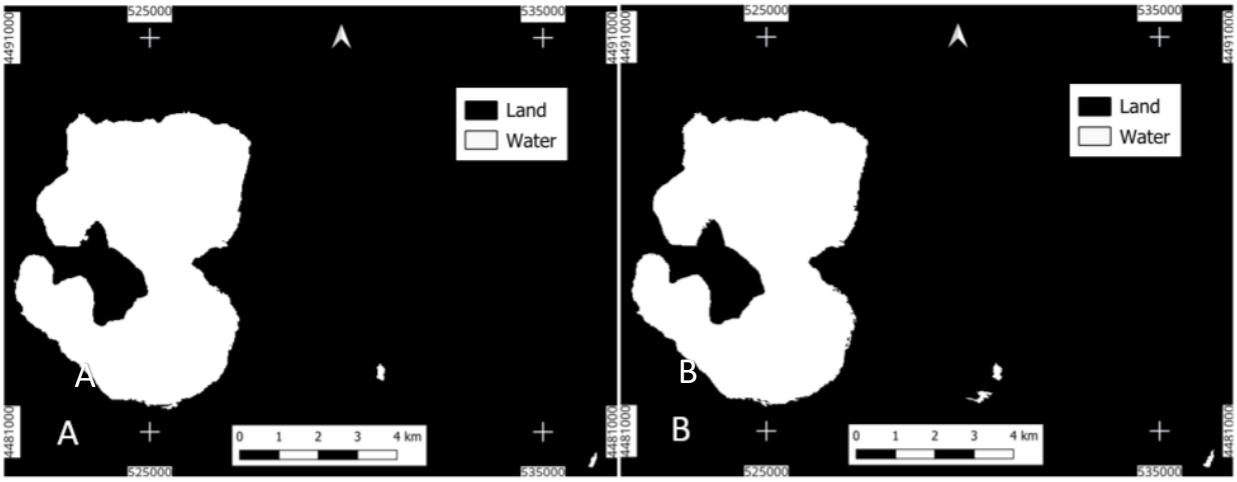

Figure 8: Examples of NDWI (a), MNDWI (b) Otsu thresholding for the same Sentinel-2 acquisition

As can be seen, besides the extent of the lake, the method has identified cloud shadows as water, which will greatly influence water area estimation. As can be seen in Figure 9, there are no other water areas nearby the lake.

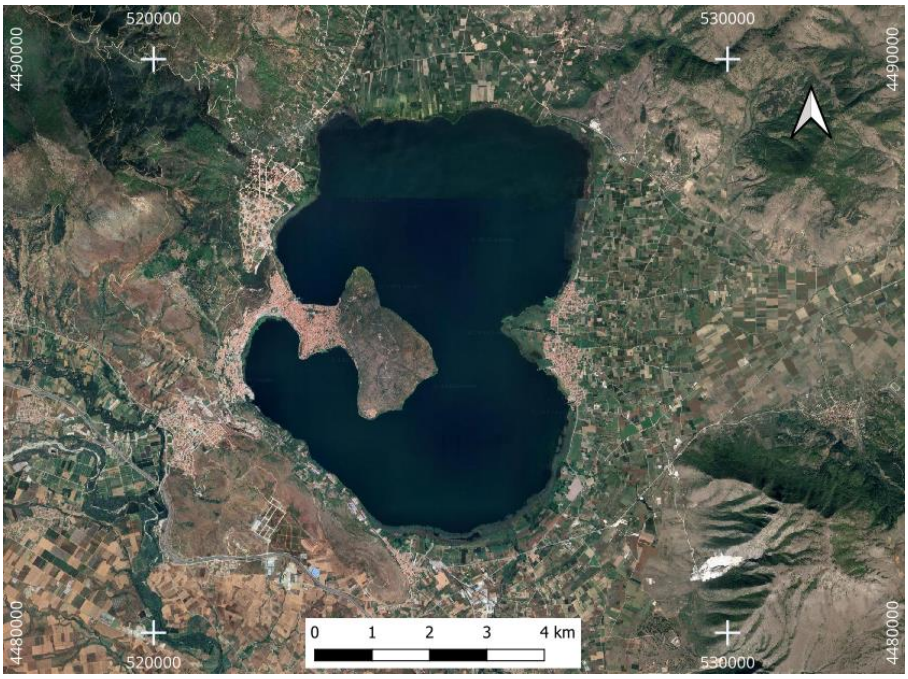

Figure 9: Aerial image of the study area, that indicates the absence of water besides the lake. Source: Google imagery 2023©

For this reason, a bounding box including the lake and nearby areas was created, so that the water area estimation will not take into consideration the false positives which are located at the right side of the lake (Figure 10)

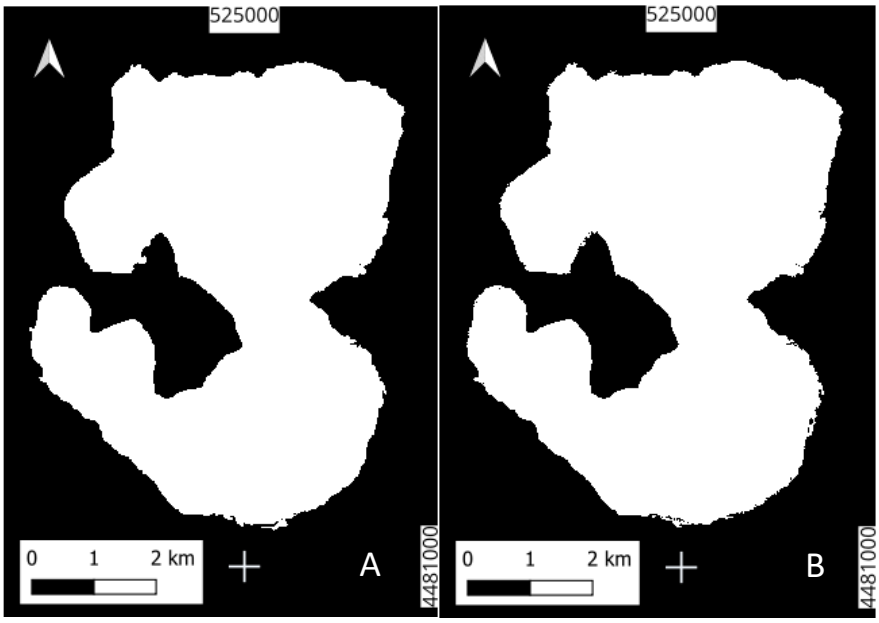

Figure 10: Cropped images of NDWI (a), MNDWI (b) Otsu Thresholding, close to the edges of the lake.

- **Random Forest**

For the machine learning part, a Random Forest algorithm has been trained, to distinguish water from land pixels. Random Forest is a supervised classifier that has been generally used for water related machine learning applications (Tyralis et al., 2019).

To construct a robust training dataset, firstly a subset of the lake was chosen for the 'water' label. Specifically, pixels from the central region of the lake were selected to ensure consistency across all images, providing a representative sample of water characteristics. Respectively, the 'land' training dataset was created with a representative bounding box that included diverse land cover types surrounding the lake. This box included various textures and land uses such as forest, urban areas, mountains, and agricultural regions, ensuring a comprehensive training 'land' label for the algorithm. The training datasets were selected to be balanced, to prevent any biases in the model and can be seen in Figure 11. Throughout the training process, multiple experiments took place, using various different parameters and options within the Random Forest algorithm with the differences in performance being marginal. Consequently, the default parameters of the algorithm, with all the spectral bands of the images were used, achieving a well-balanced and effective classification model.

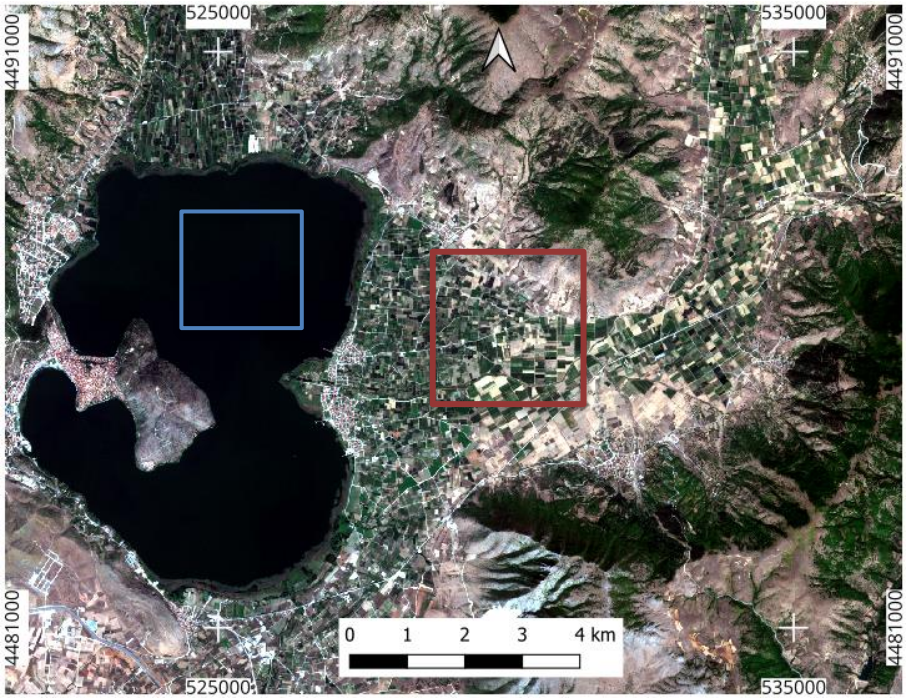

Figure 11. Water (blue) and land (red) training datasets.

An example of the predicted water no-water values of a Sentinel-2 image can be seen below (Figure 12).

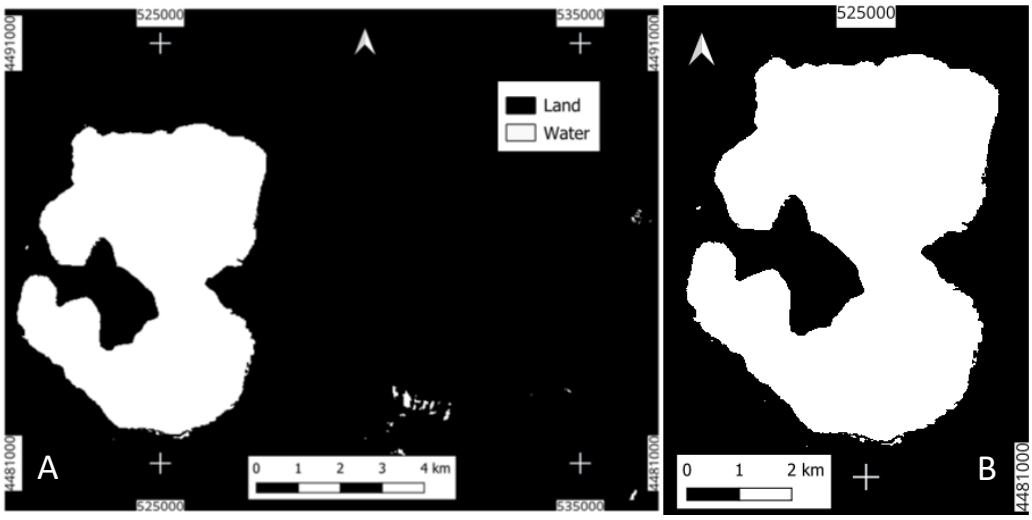

Figure 12: Example of a Random Forest predicted image (a), cropped close to the lake's edges (b).

- **Evaluation**

A quantitative comparison (accuracy assessment matrix) has taken place, comparing the test data (images created by thresholding and Random Forest) with reference data (manual digitization). For this, a function has been developed that compares the reference and estimated raster images and results in the calculation of accuracy metrics of overall accuracy, precision, recall, f1_score and kappa score:

- $Overall\ accuracy\ =\ (TP\ +\ TN)\ /\ Total$
- $Precision\ = TP\ /\ (TP\ +\ FP)$
- $Recall\ = TP\ /\ (TP\ +\ FN)$
- $F1\ score\ (weighted\ average\ of\ precision\ and\ recall)\ =$
  $2 * precision\ *\ recall\ /\ (precision\ +\ recall)$
- $Kappa\ score\ = 2\ *\ (TP * TN\ -\ FN * FP)\ /\ (TP +\ FP) * (FP + TN) + (TP + FN) * (FN + TN)$

$$TP\ =\ True\ Positives, TN\ =\ True\ Negatives, FP\ =\ False\ Positives\ and\ FN\ =\ False\ Negatives$$

True Positives are correctly predicted water pixels from the automated method compared to manual digitization, while True Negatives are correctly predicted land pixels. False Positives and False Negatives are incorrectly predicted water and land pixels.

In addition to the quantitative evaluation, a qualitative sample check took place, with several examples being manually investigated to identify differences between the automated methods results.

2.4.2 Altimetry estimation

The ICESat-2 dataset was used for the altimetry estimation of the lake. The raw heights above the Earth that the ICESat-2 dataset provides have been filtered from outliers, and the along track heights were averaged during the internal evaluation (Yuan et al., 2020).

The altimetry data have been downloaded from National Snow and Ice Data Center, n.d., accessed on 10/10/2021, according to the bounding box of the lake of interest, that was provided. A total of 54 files have been downloaded, that contained altimetry data and the orbit of ICESat-2 that crossed the bounding box of interest. In Figure 13, the altimetry measurements, that concern Kastoria Lake can be seen.

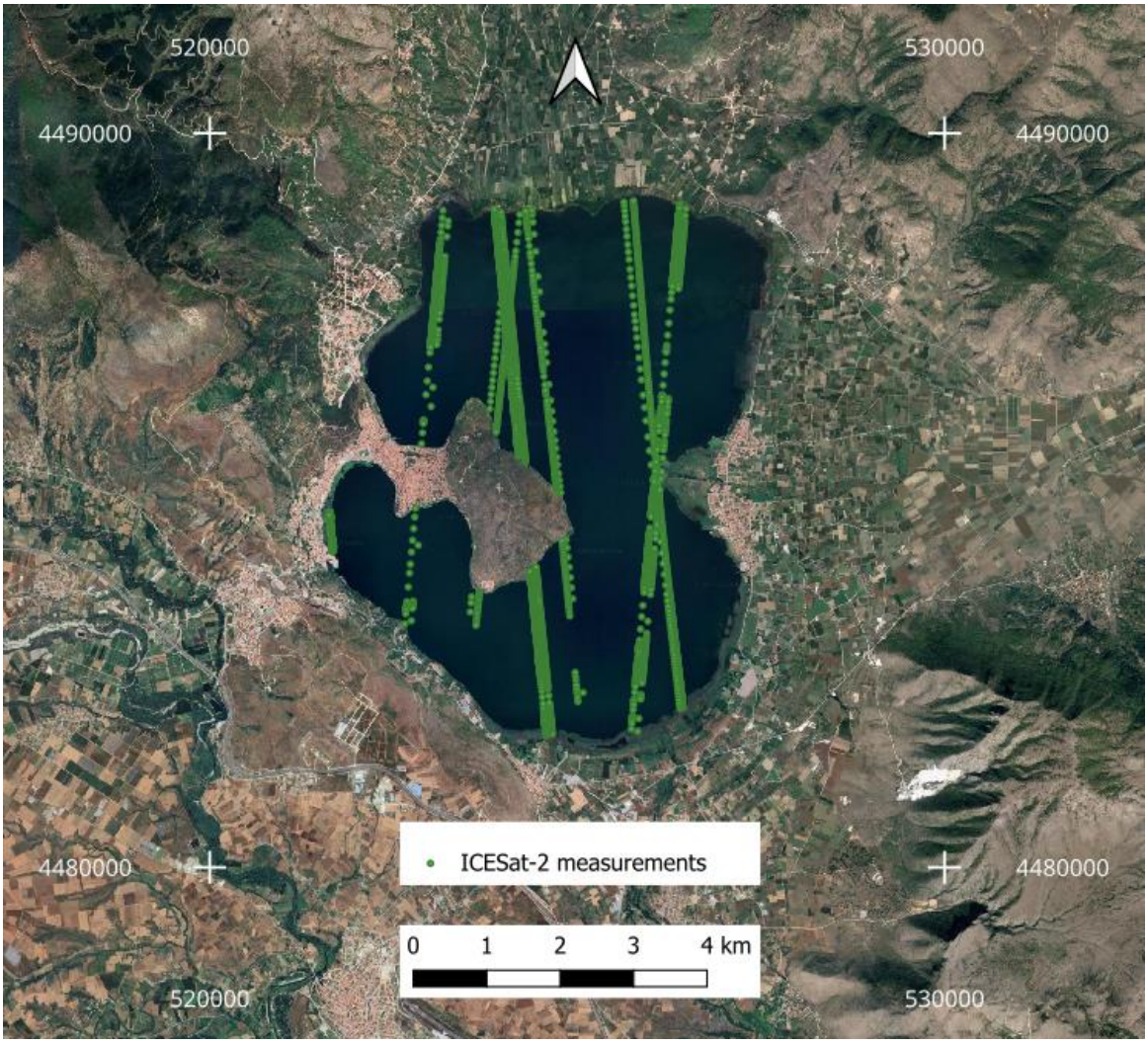

Figure 13: Visualization of ICESat-2 measurements on Kastoria Lake

According to ICESat-2 Algorithm Theoretical Basis Document (ATBD) for ATL13 version 3, (National Snow and Ice Data Center, n.d.).:

Inland water heights are processed in segments that contain a minimum of approximately 100 signal photons, to ensure the segment accurately characterizes the water surface. As such, the segments vary in length from approximately 30m to 200m (averaging about 100m), depending on factors such as signal quality and water and atmospheric conditions.

After exploring the data, in all of those beams on the available dates (54), there are 2572 measurements that have the segment id of interest and concern the 9 distinct dates of interest. For the other 45 dates, the satellite's orbit has crossed the selected bounding box but no measurements were available for Kastoria Lake. Additionally, one date was discarded because no corresponding Sentinel-2 image with low cloud coverage was available, leaving 8 available dates with corresponding altimetry measurements.

2.4.3 Water volume estimation

For the combination of the two aforementioned datasets and the water volume estimation of the lake, two methods were tested. First, a regression analysis took place with a regression equation being formed and fit along the area and elevation data, so that the area computation in the diagram will lead to the water volumes of the lake, as can be seen in Figures 14 and 15. This method requires a linear regression between the depth and area of the lake, to be applicable.

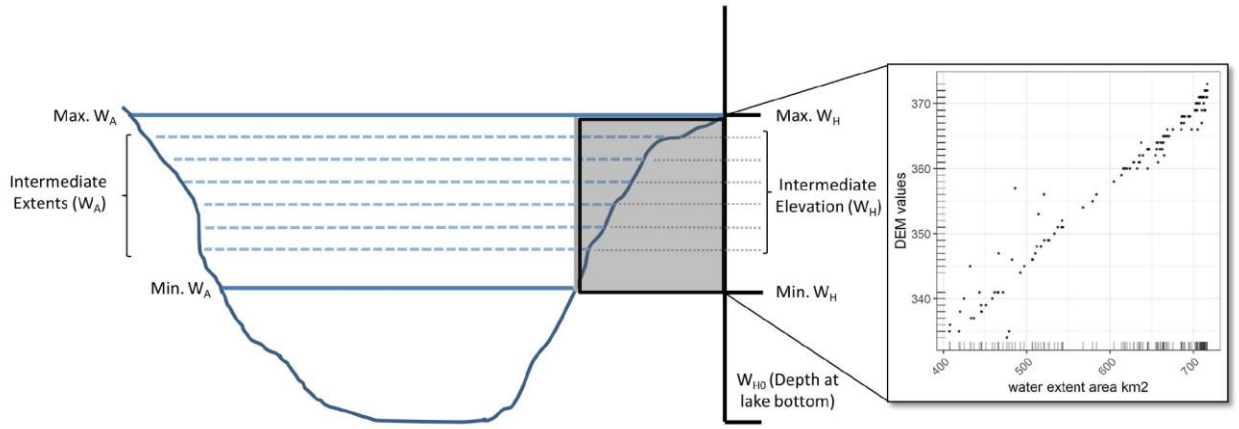

*Figure 14: A regression fit between lake areas and heights (*Bhagwat et al., 2019*). W_A denotes the water area and W_H the water height of the lake.*

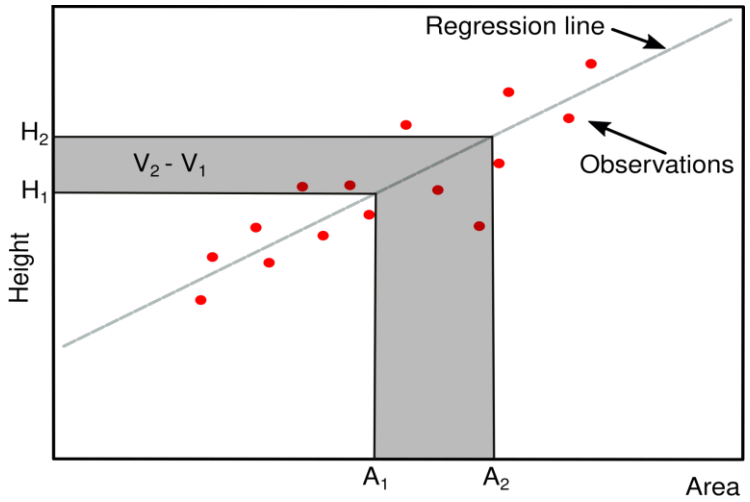

Figure 15: Volume differences as estimated from area/height pairs

According to the above, the formula for volume differences estimation between two different timestamps is:

$$V2 - V1 = ((A2 + A1) * (H2 - H1)) \ / \ 2$$

Also, a triangulated irregular network (TIN) method, was tested using QGIS and Meshlab software. This method creates triangles between the water area extents of each lake height, therefore estimating the volume directly from the created multifaceted object. Figure 16 can be further informative about this method. This method failed to produce accurate results in this case study as will be evaluated in the next chapter.

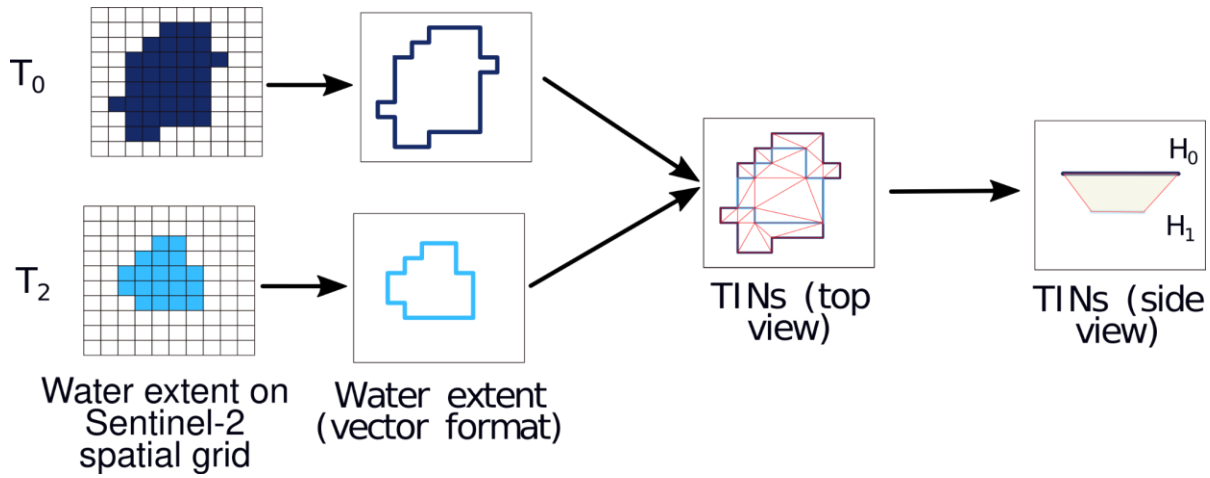

Figure 16: The TIN method for water volume estimation.

The point resolution of the produced 3D model is determined by the resolution of used multispectral imagery. In case of Sentinel-2 imagery, the resolution of the extracted water extent layer is going to be 10m. Concerning the vertical resolution of the produced 3D model, it is derived by the availability of the ICESat-2 datasets, with a pairing match of a Sentinel-2 image. More available dates of height-area pairs result in a denser produced 3D model.

Chapter 3 – Results and Discussion

3.1 Water extent estimation

3.1.1 Manual digitization - Comparison

As stated in the introduction, manual digitization was performed to create reference data in this research project. During the process, several cases have occurred, depicting peculiarities of the lake, where a human operator can distinguish the separation between water and land more accurately than automated methods. The most significant example concerns lake areas with floating vegetation, where water is present below them, but both index thresholding and machine learning approach identifies as land pixels (Figure 17).

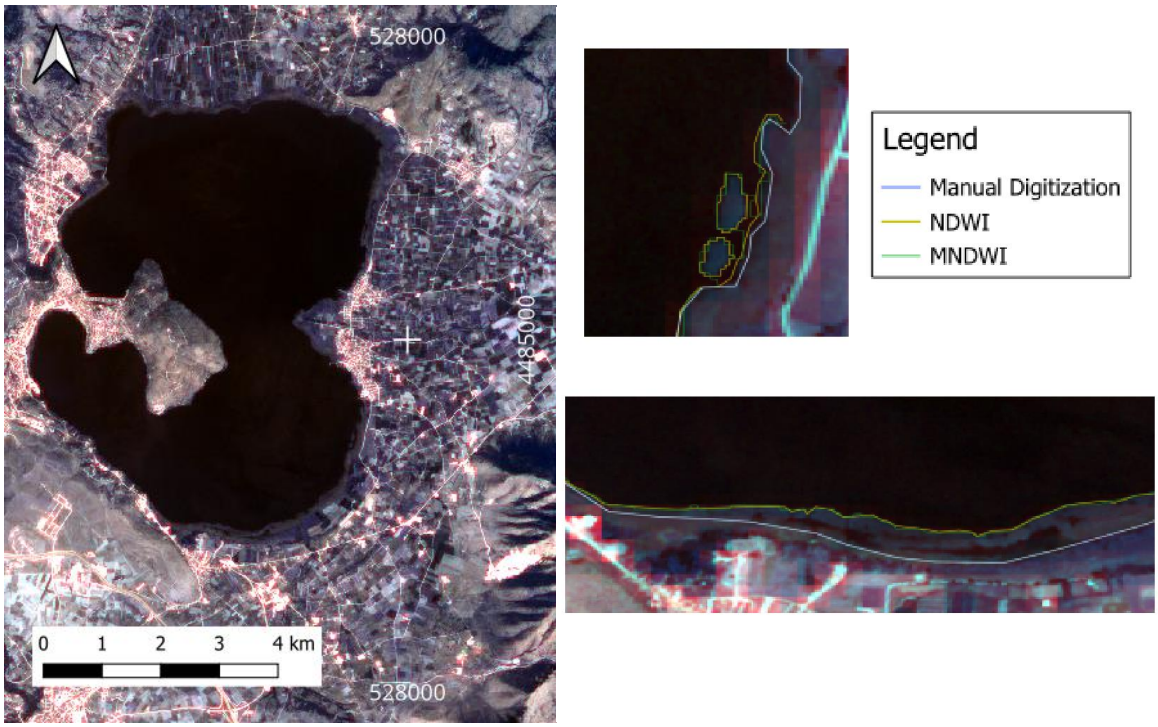

Figure 17: Examples of cases with leaves upon the water, where remote sensing indices can't recognize.

The impact of clouds is again obvious (Figure 18), besides the aforementioned cropping that took place close to the edges of the lake. Even some small clouds can be misclassified, while the shadows of those also create areas that cause problems to the automated methods.

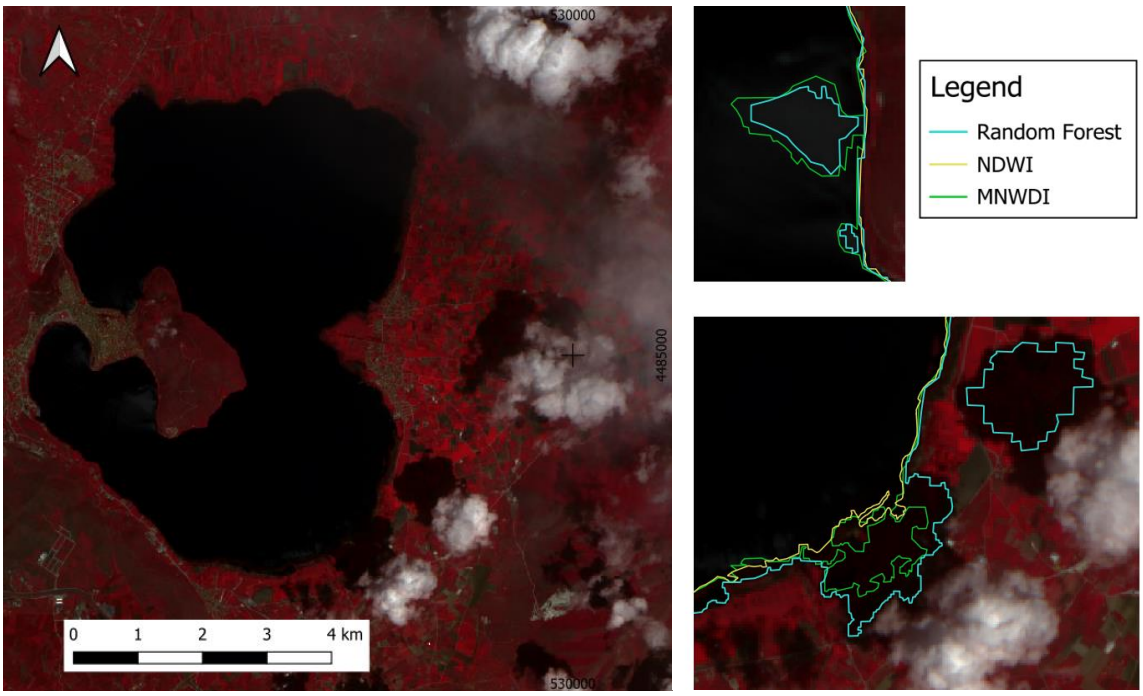

Figure 18: Examples of cloud and shadow areas that are classified inaccurate by the automated methods, but can be distinguished correctly during the manual digitization.

After careful and detailed manual digitization of all of the 30 Sentinel-2 images with low cloud coverage and visible shoreline, the water area was computed using the QGIS software package. The seasonality of the lake can be seen in Figure 19, with the water extent being lower during summer months and higher during spring. It should also be stated that the maximum spatial variation that was observed was around 30m which is considered a small variation given the spatial resolution (10m) of the Sentinel-2 imagery.

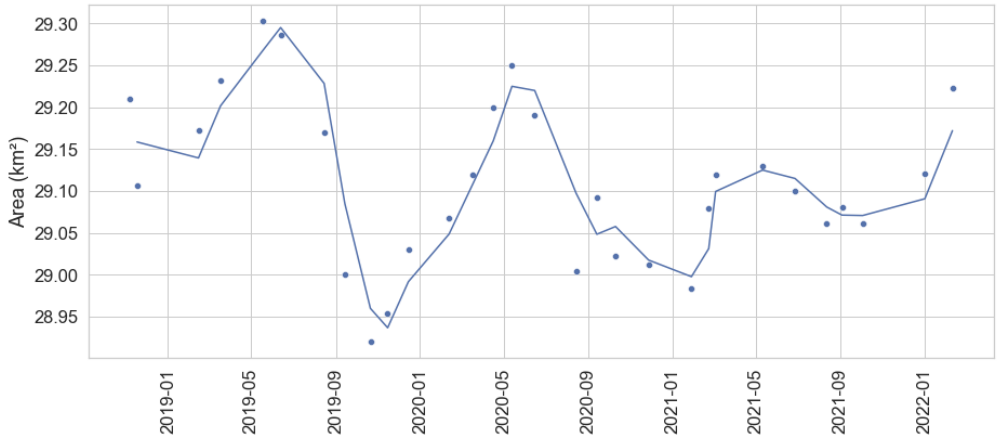

Figure 19: Lake water area over time and rolling mean (window=2), according to manual digitization.

3.1.2 Accuracy assessment

- **Quantitative comparison**

Table 1 shows the accuracy metrics of the comparison between the automated surface water area estimation methods and manual digitization, for each date.

Table 1: Table of accuracy scores of each method, compared to the reference data, per date.

	Overall Accuracy	Precision	Recall	F1 Score	Kappa Score	Date	Method
1	0.98	0.97	0.99	0.98	0.96	5/18/2019	MNDWI
2	0.98	0.97	0.99	0.99	0.97		NDWI
3	0.97	0.98	0.97	0.98	0.95		Random Forest
4	0.98	0.97	0.99	0.99	0.97	8/15/2019	MNDWI
5	0.98	0.99	0.99	0.99	0.97		NDWI
6	0.99	0.97	0.99	0.99	0.97		Random Forest
7	0.99	0.98	0.99	0.99	0.98	9/14/2019	MNDWI
8	0.99	0.98	0.99	0.99	0.98		NDWI
9	0.99	0.97	0.99	0.99	0.97		Random Forest
10	0.98	0.98	0.99	0.99	0.96	11/15/2019	MNDWI
11	0.99	0.99	0.99	0.99	0.98		NDWI
12	0.98	0.96	0.99	0.98	0.96		Random Forest
13	0.99	0.99	0.99	0.99	0.99	2/13/2020	MNDWI
14	0.99	0.99	0.99	0.99	0.99		NDWI
15	0.99	0.98	0.99	0.99	0.98		Random Forest
16	0.99	0.97	0.99	0.99	0.99	8/14/2020	MNDWI
17	0.99	0.97	0.99	0.99	0.99		NDWI
18	0.98	0.97	0.99	0.99	0.97		Random Forest
19	0.98	0.97	0.99	0.98	0.97	8/12/2021	MNDWI
20	0.98	0.97	0.99	0.99	0.97		NDWI
21	0.98	0.97	0.99	0.98	0.96		Random Forest
22	0.98	0.99	0.96	0.98	0.96	2/10/2022	MNDWI
23	0.99	0.99	0.98	0.99	0.98		NDWI
24	0.98	0.97	0.99	0.98	0.96		Random Forest

All of the metrics (Overall accuracy, Recall, Precision, F1 score, Kappa Score) were above 0.95 for all of the 3 automated methods (Figures 20, 21, and 22).

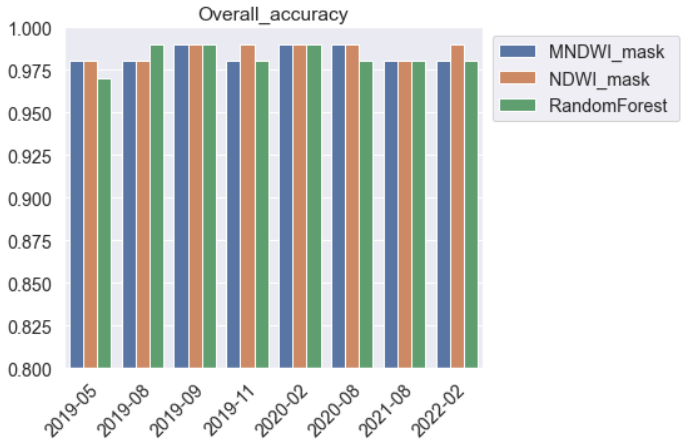

Figure 20: Overall accuracy graph

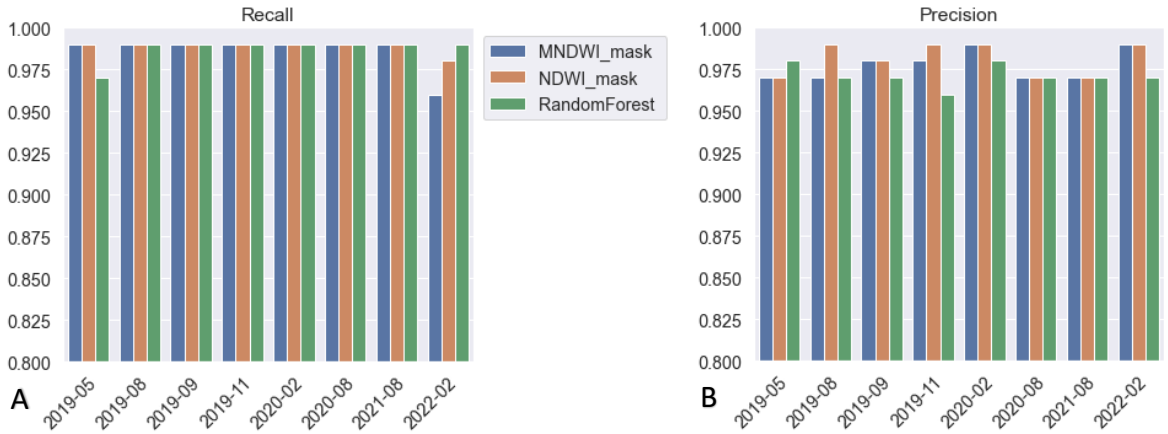

Figure 21: Recall (a) and Precision (b) graphs

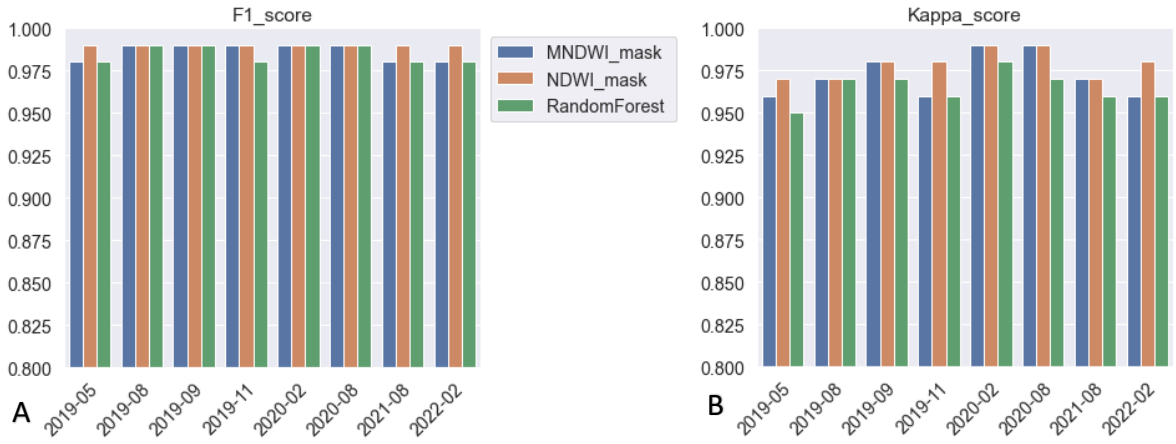

Figure 22: F1 score (a) and Kappa score (b) graphs

In this case study, the observed spatial variation of the extent of lake water over time is relatively small in comparison with the mean lake water area, which can be a possible reason for the observed high values of all the accuracy metrics.

- **Qualitative comparison**

In a qualitative assessment, several cases have occurred with misclassified small areas, mostly due to floating vegetation, clouds and shadows, as mentioned in the "Manual Digitization - Comparison" section.

Some further examples in the qualitative assessment show that besides the aforementioned cases of floating vegetation, clouds and shadows (Figure 23), all of the three methods classified water in a very similar way, with only a few pixels differing in the overall extent of the lake for the dates 17-05-2019, 14-09-2019, 14-08-2021, 17-08-2019.

Figure 23: 17-08-2019 floating vegetation area and small differences between classification methods

For 13-02-2020, Random Forest seems to have done a better job (Figures 24 and 25), while MNDWI is a bit more exaggerated, even with a small area that is totally off. NDWI has also a small offset, but is not that far off as compared to the true reference.

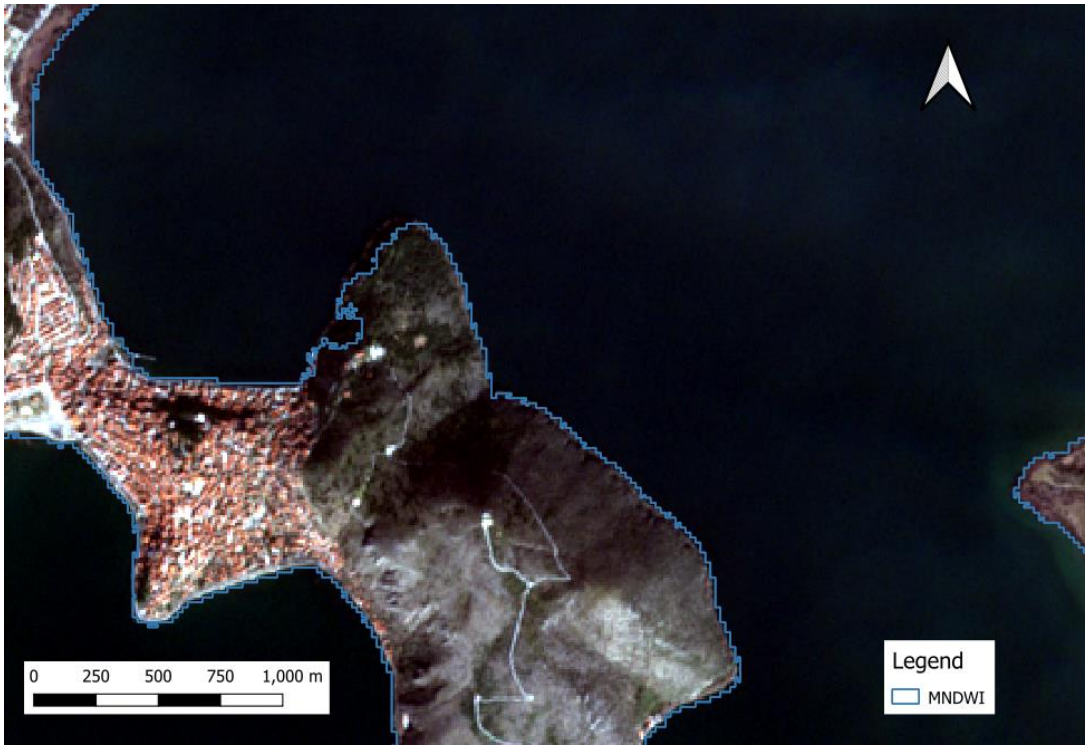

Figure 24: False Positives of MNWI for 13-02-2020

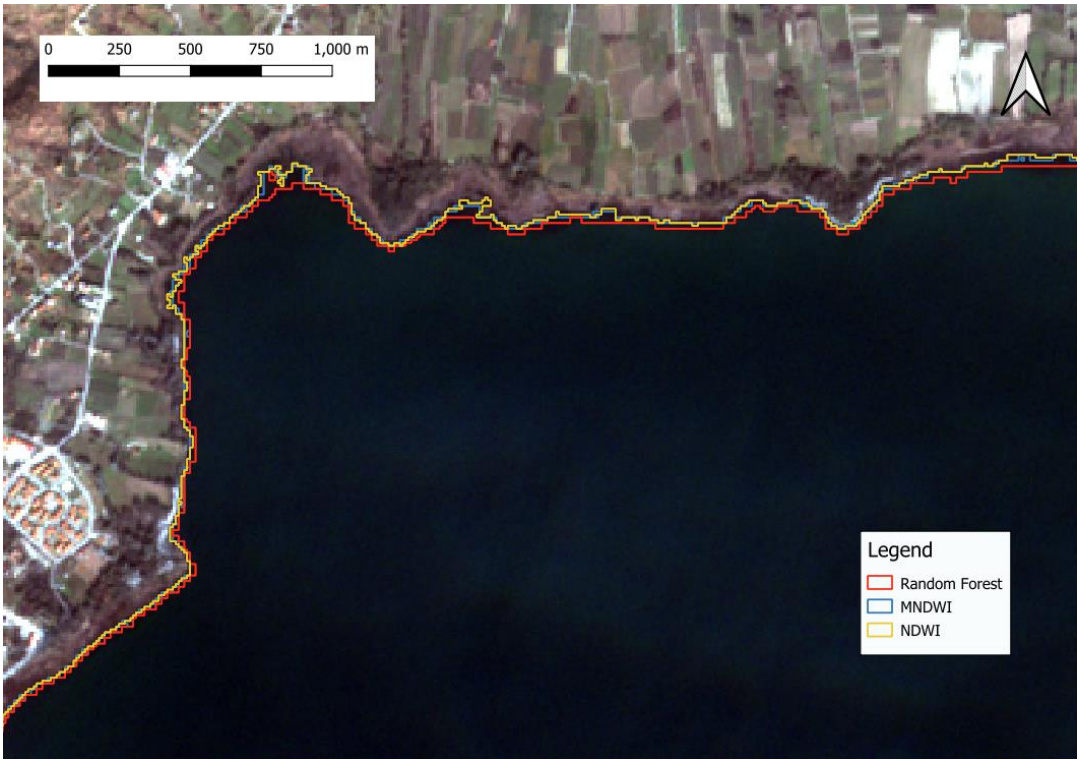

Figure 25: Small offset between NDWI and Random Forest for 13-02-2020

For 23-11-2019, NDWI and MNDWI have produced slightly better classification results for the shore of the lake, where Random Forests' shoreline is narrower (Figure 26). Yet, the indexes have also classified as water, whole areas that are outside of the lake, which outweighs the minor improvement of the shore.

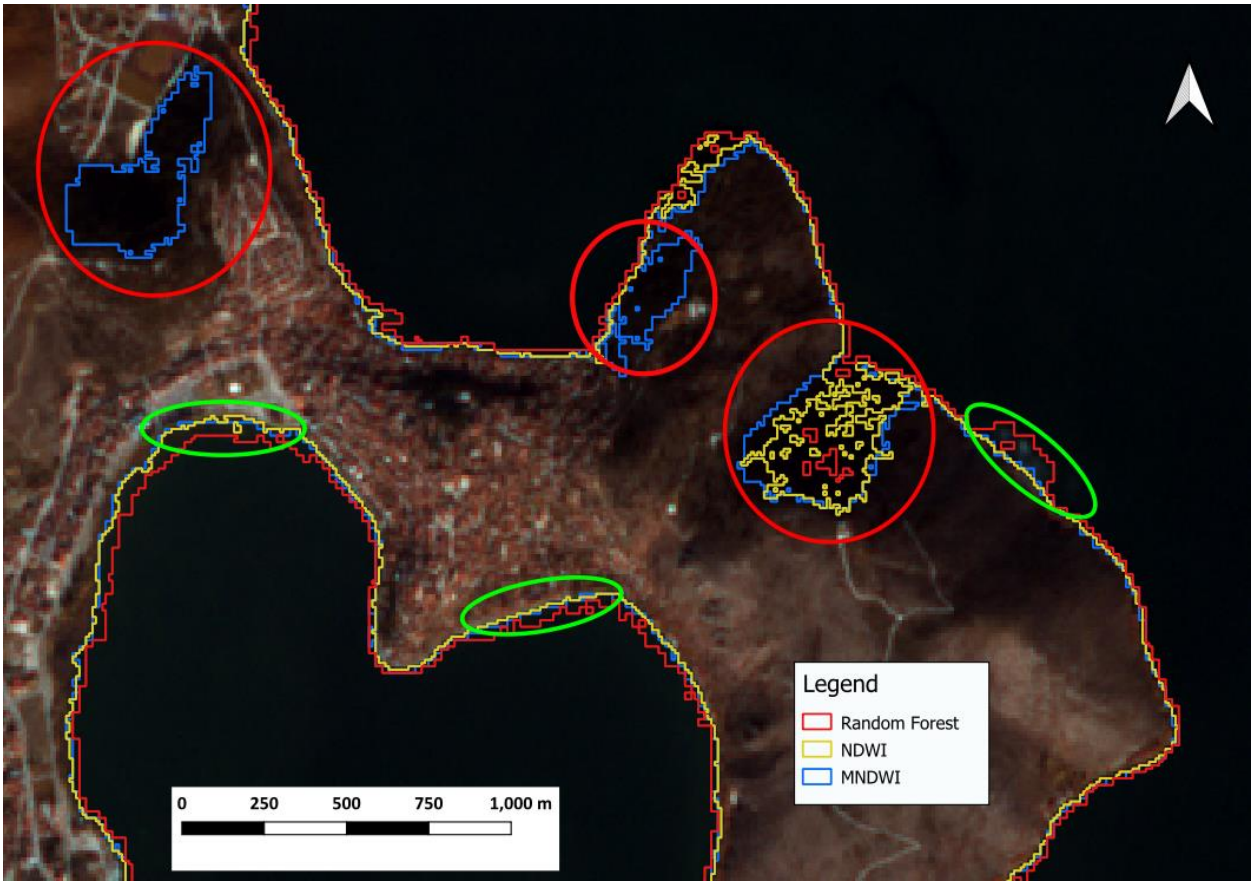

Figure 26: 23-11-2019 Winning (green circle) and losing (red circle) cases of NDWI/MNDWI against Random Forest

The same is the case for 10-02-2022, with the indices matching more accurately the shoreline, yet overestimating whole areas totally outside the lake, which are not water according to inspection by human eye (Figure 27).

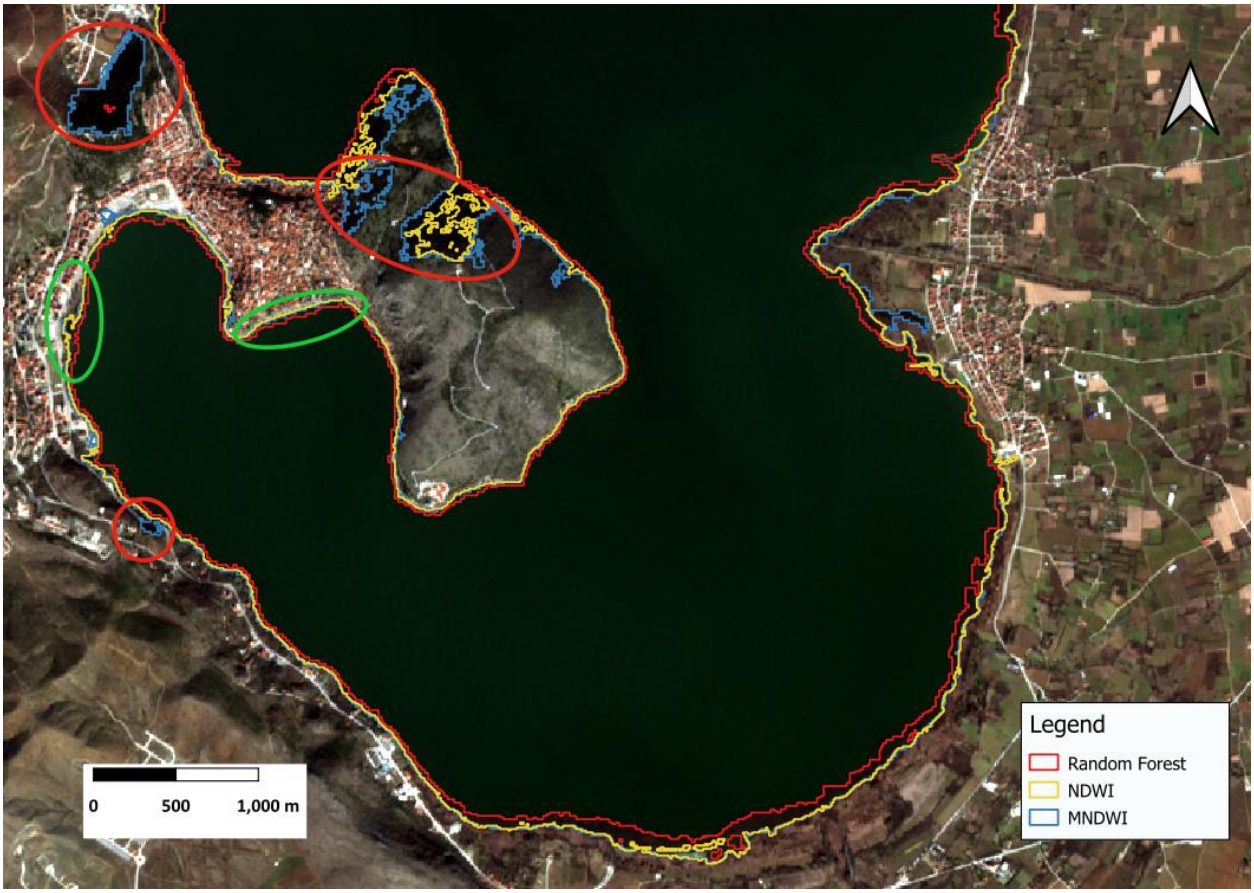

Figure 27: Matched and mismatched cases of NDWI/MNDWI against Random Forest for 10-02-2022

Considering the above examples per specific date, it seems that the indices have been a bit more conservative when trying to classify water pixels. There were cases of minor improvement alongside the shoreline, but there were also much bigger areas being misclassified, probably due to shadows that were interpreted as water, which is a case where Random Forest had better performance. Overall, the presence of leaves upon the lake makes the process very difficult for automated algorithms, even for the human eye in many cases, to fully accurately map the water extent.

3.2 Water level estimation

In Figure 28, all the available measurements from the ICESat-2 datasets can be seen. The dataset seems robust, with only a few outliers. Specifically, only for 2020-02-12 two significant outliers have been identified, that were deleted before the average water level calculation per date. Moreover, we can observe that on 2019-09, 2020-02 and 2020-08 we have higher variation of ICESat-2 observations, compared to the other dates. However, even for those dates the standard deviation ($\sim 5\text{cm}$) is considered satisfactory given the nominal accuracy of 6.1 cm. The fact that each date contains lots of measurements that are close to each other shows that the dataset is precise, can be trusted and further used for this case study. A downside of the dataset is that from the 54 available files that were downloaded, according to the provided bounding box, only 9 had indeed data for the area of interest, since for the rest of them, the trajectory of the satellite indeed passed by the area, but there were no altimetry data for Kastoria Lake.

Figure 28: Distribution of ICESat-2 water level values at selected dates

Ideally, more distinct dates would be needed to study the seasonality of the lake's altimetry, yet it can be seen that there are low height values in the summer months and winter, while the peak is during May. The mean values and standard deviations of the above measurements, after outlier cleaning, grouped by the distinct dates, is available in Figure 29, where it can be seen that the maximum elevation difference is ~50cm. We can also observe that the mean elevation differences between consecutive dates are larger than the actual precision (standard deviation) for all cases, expect for the 09/2019 -11/2019 pair.

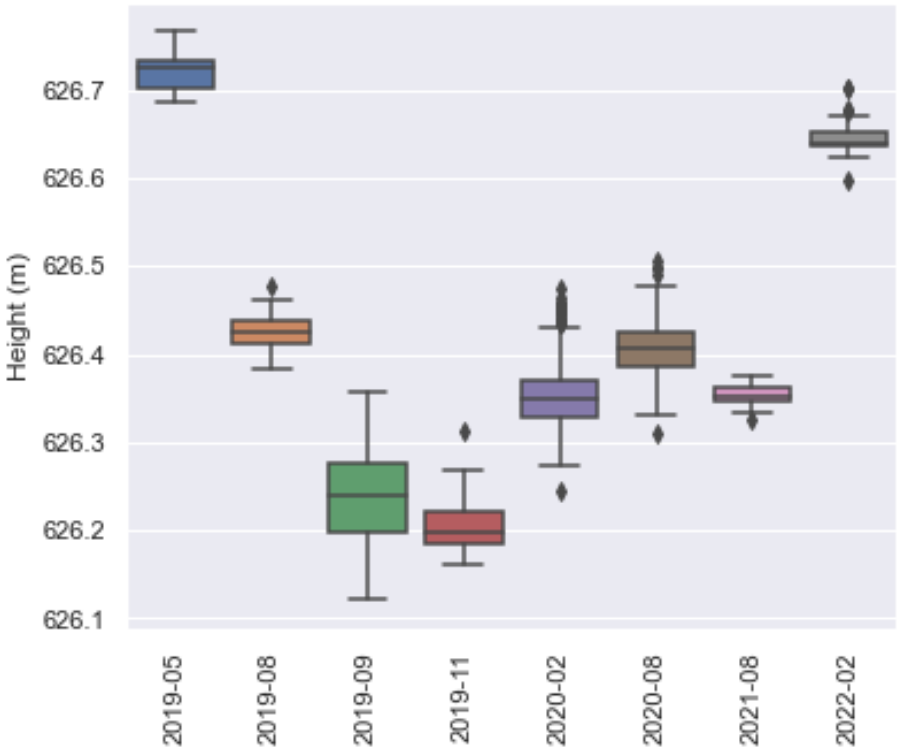

Figure 29: Boxplot of lake height values per date of clean altimetry dataset.

Concerning the applicability of ICESat-2 data, the main disadvantage is the actual availability of information for a specific area of interest. The main advantage is that they are openly available data, that can be used by anyone with no cost. Ideally, there would be available ground truth to thoroughly test the accuracy, yet even with the low number of available dates, the results seem to be precise and robust, therefore suitable for such applications. In this case study, the mean calculated precision (~5cm) of the ICESat-2 data was found satisfactory in relationship with the reported nominal accuracy by the National Snow and Ice Data Center (n.d.) (6.1 cm).

3.3 Water Volume fluctuations estimation

3.3.1 Regression

The area, as calculated from the manual digitized shapefiles has been plotted alongside with the altimetry data from ICESat-2 as shown in the following plot (Figure 30).

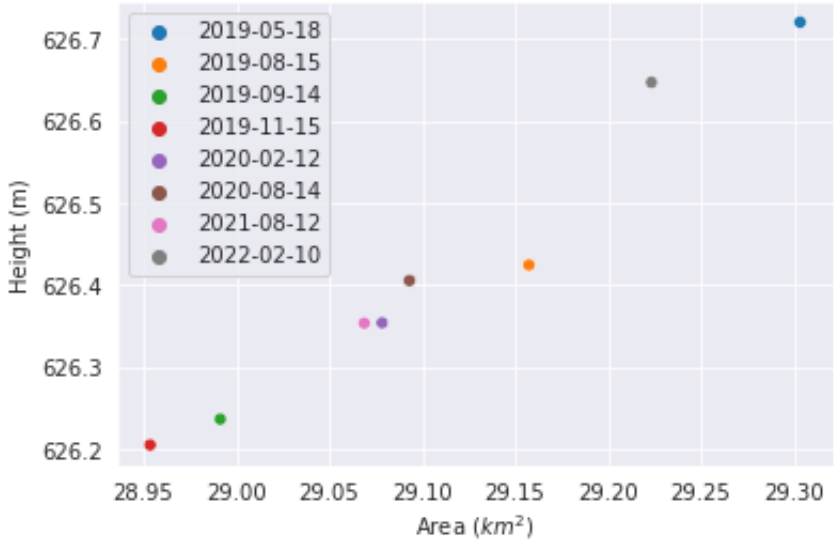

Figure 30: Area vs height plot of Kastoria lake

R-squared was estimated to be 0.96. By fitting a linear regression (Figure 31), the factors are: slope=1.54e-06, intercept=581.70, r-value=0.98, p-value=1.63e-05.

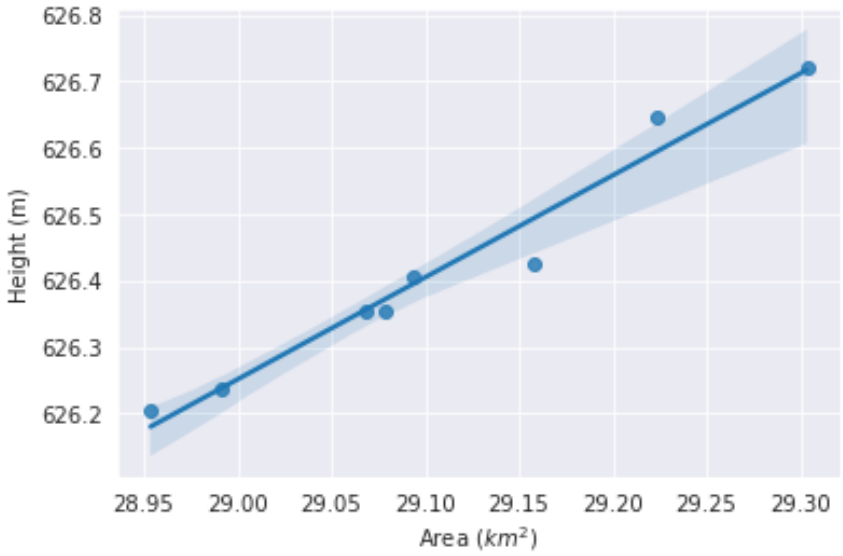

Figure 31: Linear Regression line, depicting the correlation between water area and height of the lake

Volume differences can be estimated from the regression graph, according to the area of the trapezoid, as shown in the image below (Figure 32).

Considering the first date 2019-05-18, where the area and height values are the highest, as a starting point with V=0 km^3, the water volume changes can be estimated for the following dates.

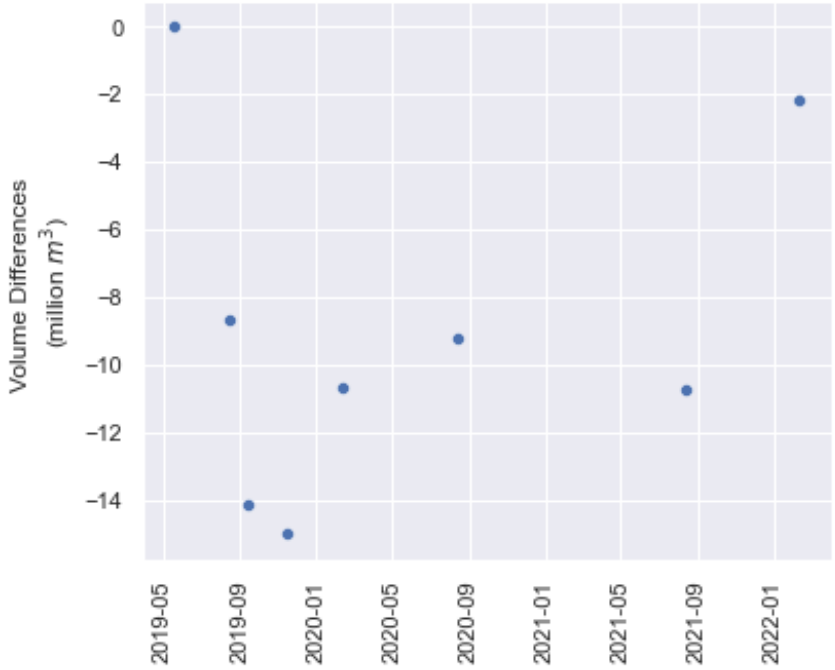

Figure 32: Sequential volume differences over time

3.3.2 Triangulated Irregular Network (TIN)

For the TIN method, two implementations were tested. The first one is provided from QGIS software and the second one from the Meshlab software package.

Firstly, QGIS software has been used with the TIN interpolation tool. There, the input data were the points of each date's digitization polygon of lake's extent with the corresponding ICESat-2 altimetry measurement. For each pair of dates, the TINs were created, to estimate the volume of the 3D object.

Yet, according to the experiments, the method doesn't work for the specific case study. Each date is considered to be a surface, since all the digitized points of the shoreline have the same height. In that way, the created TINs were expected to just connect the outer points of the shoreline of each date's polygon with the closest ones of the other date's shapefile. In the following screenshots of the created TINs from QGIS, the shapes are not explainable. The software has connected nodes from completely different parts of the lake, while the final shape does not have the shape of a parallelepiped (Figure 33).

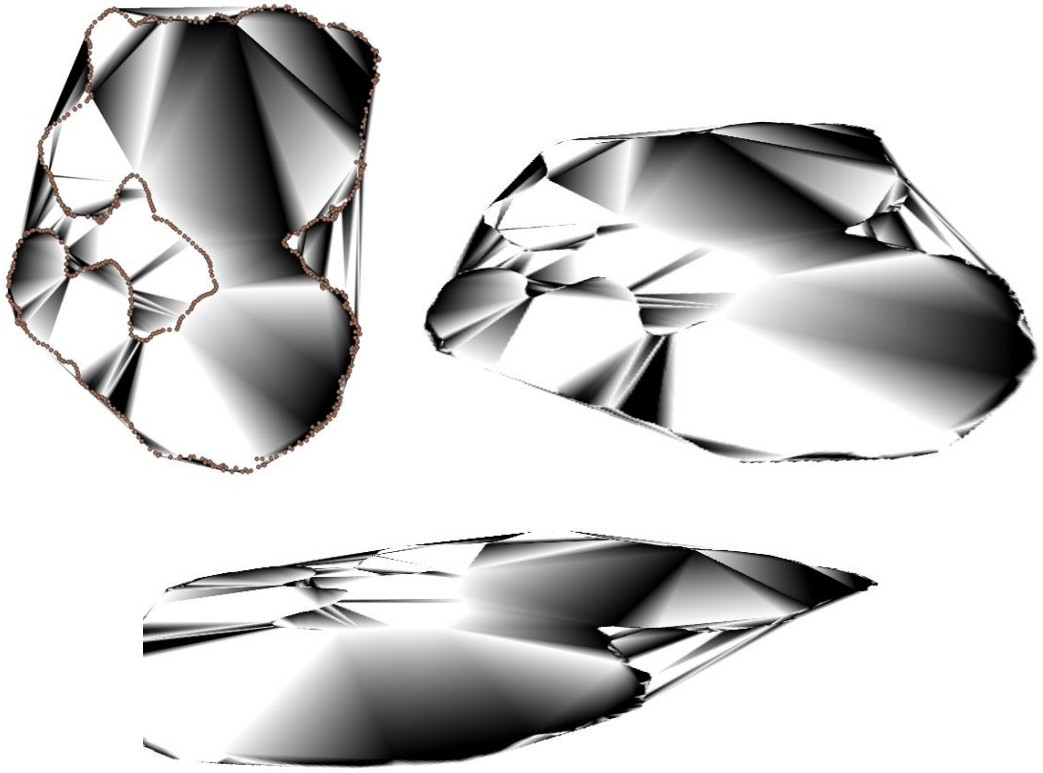

Figure 33:
Different angles of the produced TINs by qGIS software. It can be seen that the algorithm has not worked as expected, since the produced object does not have the shape of a parallelepiped.

The procedure was also applied in Meshlab software with a similar TIN creation algorithm and the results were again not as expected. The connection of the nodes has not been done in a way that can be further utilized to estimate the volume of the geometric object (Figure 34).

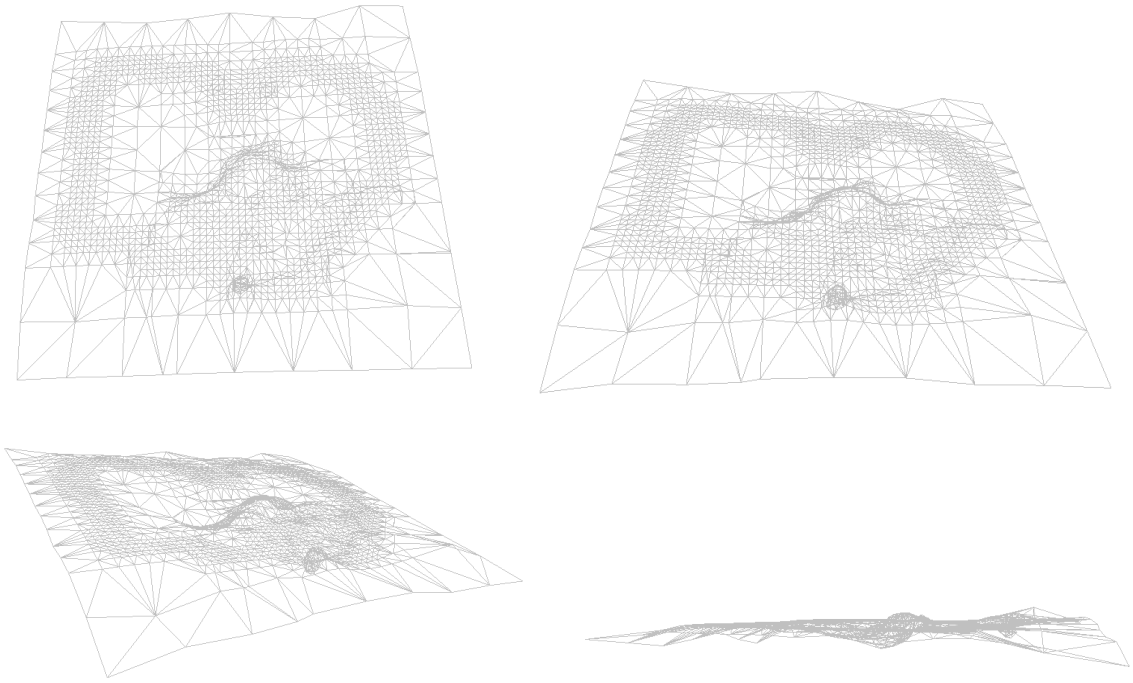

Figure 34:
Different angles of the produced TINs by Meshlab software. The results are similar with QGIS and indicate that this methodology cannot be utilized for the specific case study.

A possible explanation for the failure of this method has to do with the vertical scale of the points, compared to the horizontal one. The maximum height difference that was met in the dataset was some centimeters, while the vertical resolution of Sentinel-2 imagery is 10x10m (order of meters). This creates an inconsistency between the z and x-y axes which concludes in the unusable created TINS.

3.4. Discussion

In this thesis, a 3-step methodological approach to extract lake water volumes that is based on open-source software tools (e.g., python functionalities, QGIS) and free satellite data (Sentinel-2, ICESat-2) is presented. In the first step, the lake water area estimation is performed with Sentinel-2 data. In the second step, the lake water level estimation is performed with ICESat-2 data. In the third step, the lake water area and level estimation were exploited to calculate lake water volume changes with regression-based and TIN-based methodologies. The aforementioned approach could greatly benefit a range of stakeholders, including decision makers, local communities, and water organizations, at low or no cost.

The methodology used in this study makes use of free, open data, and can also be modified to support other open-source data, such as Landsat 8/9. Even though in this case study there were only 8 available pairs between Sentinel-2/ICESat-2, future initiatives will ensure the continuity of the data, and it is expected to have access to more data pairs. The proposed methodology can also be applied to other altimetry data, such as Jason-2, a U.S.-European series of satellite missions designed to measure sea surface height (JPL, Jason2, retrieved on 03-12-2023), and also in-situ data from large lakes can be used for validation purposes. The study makes use of open-source software and tools, and suggest a framework that can be used for future research, education, and to gain insights into water volume monitoring from space.

The water extent mapping methods used in this study showed good accuracy overall, with data-driven approaches having the greatest potential for improvement in general (Neumann et al., 2021). All of the 3 methods provided reasonably accurate results, since the problem was not too complex for the machine learning techniques employed, as the metrics show. With all the accuracy metrics being above 0.95, which are considered very good scores, there does not seem to be a clearly preferred method amongst the set of quantitative approaches. The actual performance of each method should be further examined in another case study with a set of lakes with larger seasonal spatial variations (Ma et al., 2019). Other limitations related to misclassifications, spatial resolution, and the effects of clouds and shadows were identified, and the use of active remote sensing data such as SAR data can help overcome those (Marzi & Gamba, 2021). The maximum observed spatial variation of Kastoria Lake was around 30m which is considered small, given that the minimum spatial resolution of Sentinel-2 imagery is 10m, with SWIR band (used in MNDWI index) being 20m. This minimal change in spatial water variations has also caused problems with the TINs creation. In future work, more sophisticated data-driven approaches such as convolutional neural networks towards semantics segmentation (Li et al., 2019), or water detection (Wang et al., 2020) can be incorporated, to improve the solution. -

The ICESat-2 datasets were found to be a suitable choice for estimating water level with an observed overall precision of ~5 cm, which is better than the reported nominal accuracy of 6.1 cm (National Snow and Ice Data Center. n.d.). For the all the consecutive dates, we observed larger lake height changes compared to the estimated precision, expect for the case of 09/2019 - 11/2019 pair. However, the absence of ground measurements prevents us from being able to

discuss on absolute accuracy. Also, the poor temporal resolution and inconsistent data acquisition were limitations in this study. This affects the combinatory analysis with Sentinel-2 acquisitions, since in this case study, only 8 usable pairs were exploited. The use of several altimetry datasets from various sources, such as Jason-2, should be considered in future work (Birkett & Beckley, 2010).

The regression modeling used in this study provided satisfactory results for water volume estimation, while TINs were not effective with a possible reason of different scale of vertical and horizontal changes. Lu et al. (2013) in their research, used a methodology based on TINs as well, with the height differences between the measurement's dates being within the scale of some meters, which could make a significant difference for the algorithm. Kastoria Lake that has been studied in this research, seems to have some geometric particularities concerning its sensitivity to height and extent differences that do not allow the TINS algorithm to generate accurate results. Although TINs were not applicable in this case, they may be a suitable alternative in other cases where spatial variations are comparable to vertical ones, such as Lu et al. (2013) case. Unfortunately, a comparison between the two proposed methods for water volume estimation was not possible due to the limitations of the TIN approach.

Chapter 4 - Conclusion

In conclusion, the next three paragraphs will address the research questions that concern the estimation of the water area from optical satellite imagery, the extraction of water level using satellite altimetry data and the combination of spatial and height to obtain volumetric differences.

For the first objective related to the accuracy assessment of water spatial extent estimations extracted from NDWI and MNDWI remote sensing indexes and machine learning, in respect to water spatial extent extracted by manual digitization of Sentinel-2 satellite imagery, all of the 3 methods provided reasonably accurate results, having >0.95 in all performance metrics, so there does not seem to be a clearly preferred method amongst the set of quantitative approaches.

For the second objective, related to the potential use of ICESat-2 satellite observations in lake water level monitoring, the results were encouraging when it comes to the precision of the lake water level observations. The precision expressed by the standard deviation in this case study was ~5 cm, which is considered acceptable given the nominal accuracy of 6.1 cm. (National Snow and Ice Data Center. n.d.). However, concerning their temporal frequency, the temporal resolution was found poor which was a limitation in this study, since it affected the combinatory analysis with Sentinel-2 acquisitions.

Finally, for the third objective of comparing the results between regression and GIS-generated TINs, it was found that the latter didn't produce satisfactory results for this case study, due to the scale difference between horizontal and vertical changes in the Kastoria Lake so the comparison could not be performed. According to the results the regression method may be better applicable to lakes that have different scale of vertical and horizontal changes.

Bibliography

Bhagwat, T., Klein, I., Huth, J., & Leinenkugel, P. (2019). Volumetric analysis of reservoirs in drought-prone areas using remote sensing products. *Remote Sensing*, *11*(17), 1–20. https://doi.org/10.3390/rs11171974

Birkett, C. M., & Beckley, B. (2010). Investigating the Performance of the Jason-2/OSTM Radar Altimeter over Lakes and Reservoirs. *Marine Geodesy*, *33*, 204–238. https://doi.org/10.1080/01490419.2010.488983

Busker, T., De Roo, A., Gelati, E., Schwatke, C., Adamovic, M., Bisselink, B., Pekel, J. F., & Cottam, A. (2019). A global lake and reservoir volume analysis using a surface water dataset and satellite altimetry. *Hydrology and Earth System Sciences*, *23*(2), 669–690. https://doi.org/10.5194/hess-23-669-2019

Du, Y., Zhang, Y., Ling, F., Wang, Q., Li, W., & Li, X. (2016). Water bodies' mapping from Sentinel-2 imagery with Modified Normalized Difference Water Index at 10-m spatial resolution produced by sharpening the swir band. *Remote Sensing*, *8*(4). https://doi.org/10.3390/rs8040354

Duan, Z., & Bastiaanssen, W. G. M. (2013). Estimating water volume variations in lakes and reservoirs from four operational satellite altimetry databases and satellite imagery data. *Remote Sensing of Environment*, *134*, 403–416. https://doi.org/10.1016/j.rse.2013.03.010

Fluet-Chouinard, E., Messager, M. L., Lehner, B., & Finlayson, C. M. (2017). Freshwater Lakes and Reservoirs. In *The Wetland Book* (pp. 1–18). Springer Netherlands. https://doi.org/10.1007/978-94-007-6173-5_201-2

Gabila Buma, W., Lee, S.-I., & Seo, J. Y. (n.d.). *Recent Surface Water Extent of Lake Chad from Multispectral Sensors and GRACE*. https://doi.org/10.3390/s18072082

Gianneli E. (2009), Hydrogeology investigation of basins of Greece: example from the basin of Agioi Anargiroi, Kastoria, Dissertation, Aristotle University of Thessaloniki. (in Greek).

Hemalatha, M. (2021). Water Feature Extraction, Enhancement and Change Detection of Multi-Temporal Satellite Images using MNDWI2-PCA. *IOP Conference Series: Materials Science and Engineering*, *1049*(1), 012005. https://doi.org/10.1088/1757-899x/1049/1/012005

Herndon, K., Muench, R., Cherrington, E., & Griffin, R. (2020). An assessment of surface water detection methods for water resource management in the Nigerien Sahel. Sensors (Switzerland), 20(2), 1–14. https://doi.org/10.3390/s20020431

Karamoutsou, L., & Psilovikos, A. (2021). Deep learning in water resources management: The case study of Kastoria lake in Greece. Water (Switzerland), 13(23). https://doi.org/10.3390/w13233364

Jet Propulsion Laboratory (JPL) - NASA. Jason-2: NOAA/NASA Satellite. https://www.jpl.nasa.gov/missions/jason-2 accessed on 2023-12-03

Lakes / Orestiada-lake, NaturaGraeca. (n.d.). Retrieved February 8, 2021, from https://www.naturagraeca.com/ws/129,191,115,2,1,Orestiada-lake

Li, Z., Wang, R., Zhang, W., Hu, F., & Meng, L. (2019). Multiscale features supported deeplabv3+ optimization scheme for accurate water semantic segmentation. IEEE Access, 7, 155787–155804. https://doi.org/10.1109/ACCESS.2019.2949635

Lu, S., Ouyang, N., Wu, B., Wei, Y., & Tesemma, Z. (2013). Lake water volume calculation with time series remote-sensing images. *International Journal of Remote Sensing*, *34*(22), 7962–7973. https://doi.org/10.1080/01431161.2013.827814

Ma, Y., Xu, N., Sun, J., Wang, X. H., Yang, F., & Li, S. (2019). Estimating water levels and volumes of lakes dated back to the 1980s using Landsat imagery and photon-counting lidar datasets. *Remote Sensing of Environment*, *232*, 111287. https://doi.org/https://doi.org/10.1016/j.rse.2019.111287

Marzi, D., & Gamba, P. (2021). Inland Water Body Mapping Using Multitemporal Sentinel-1 SAR Data. *IEEE Journal of Selected Topics in Applied Earth Observations and Remote Sensing*, *14*, 11789–11799. https://doi.org/10.1109/JSTARS.2021.3127748

Matzafleri, N., Magnisia, P., Margoni, S., Psilovikos, A., Matzafleri, N., Margoni, S., & Psilovikos, A. (2009). *Assessment of Water Quality Monitoring Data in Lake Kastoria, Western Macedonia, Greece*. https://www.researchgate.net/publication/320403816

Neumann, A., Dong, F., Shimoda, Y., Arnillas, C. A., Javed, A., Yang, C., Zamaria, S., Mandal, S., Wellen, C., Paredes, D., Feisthauer, N., Blukacz-Richards, E. A., Yerubandi, R. R., & Arhonditsis, G. B. (2021). A review of the current state of process-based and data-driven modelling: Guidelines for lake erie managers and watershed modellers. In *Environmental Reviews* (Vol. 29, Issue 4, pp. 443–490). Canadian Science Publishing. https://doi.org/10.1139/er-2020-0070

Otsu. N, A threshold selection method from gray-level histograms. IEEE Transactions on Systems, Man and Cybernetics, Vol.9, No.1, (1979), P.62-66.

PDM – Region of Western Macedonia https://www.pdm.gov.gr/enimerosi-ependyton/ydatinoi-poroi/oikosystimata-kai-prostateyomenes-perioches/, accessed on 2022-08-02

Smith, B., Fricker, H. A., Holschuh, N., Gardner, A. S., Adusumilli, S., Brunt, K. M., Csatho, B., Harbeck, K., Huth, A., Neumann, T., Nilsson, J., & Siegfried, M. R. (2019). Land ice height-retrieval algorithm for NASA's ICESat-2 photon-counting laser altimeter. *Remote Sensing of Environment*, *233*. https://doi.org/10.1016/j.rse.2019.111352

Tyralis, H., Papacharalampous, G., & Langousis, A. (2019). A brief review of random forests for water scientists and practitioners and their recent history in water resources. *Water (Switzerland)*, *11*(5). https://doi.org/10.3390/w11050910

Tzampoglou, P., Ilia, I., Karalis, K., Tsangaratos, P., Zhao, X., & Chen, W. (2023). Selected Worldwide Cases of Land Subsidence Due to Groundwater Withdrawal. In *Water (Switzerland)* (Vol. 15, Issue 6). MDPI. https://doi.org/10.3390/w15061094

Voulanas D, Theodossiou N, & Hatzigiannakis E. (2021). Assessment of potential hydrological climate change impacts in Kastoria basin (Western Macedonia, Greece) using EUROCORDEX regional climate models. *Global NEST Journal*. https://doi.org/10.30955/gnj.003444

Wang, G., Wu, M., Wei, X., & Song, H. (2020). Water identification from high-resolution remote sensing images based on multidimensional densely connected convolutional neural networks. *Remote Sensing*, *12*(5). https://doi.org/10.3390/rs12050795

Yuan, C., Gong, P., & Bai, Y. (2020). Performance assessment of ICESat-2 laser altimeter data for water-level measurement over lakes and reservoirs in China. *Remote Sensing*, *12*(5). https://doi.org/10.3390/rs12050770

Appendix

Code segments

Water extent estimation functionalities

Dictionary of the satellite's bands

```
Dict_S2={'B01':0,
   'B02':1,
   'B03':2,
   'B04':3,
   'B05':4,
   'B06':5,
   'B07':6,
   'B08':7,
   'B08A':8,
   'B09':9,
   'B10':10,
   'B11':11,
   'B12':12}
```

Function to compute MNDWI values of each pixel

```
#MNDWI
def _compute_10m_mndwi(S2_image):

  '''
  Du, Y.; Zhang, Y.; Ling, F.; Wang, Q.; Li, W.; Li, X. Water Bodies' Mapping
  from Sentinel-2 Imagery with Modified Normalized Difference Water Index at
  10-m Spatial Resolution Produced by Sharpening the SWIR Band.
  Remote Sens. 2016, 8, 354.
  '''

  # Read image as array
  S2_image_data=gdal.Open(S2_image).ReadAsArray().astype(np.float)

  # Estimate MNDWI pixel values
  mndwi_10m=np.divide((S2_image_data[Dict_S2['B03'],:,:]-
S2_image_data[Dict_S2['B11'],:,:]),(S2_image_data[Dict_S2['B03'],:,:]+S2_i
mage_data[Dict_S2['B11'],:,:]))

  del S2_image_data

  return mndwi_10m
```

Function to compute NDWI values of each pixel

```
#NDWI
def _compute_10m_ndwi(S2_image):

  '''
  Du, Y.; Zhang, Y.; Ling, F.; Wang, Q.; Li, W.; Li, X. Water Bodies' Mapping
  from Sentinel-2 Imagery with Modified Normalized Difference Water Index at
  10-m Spatial Resolution Produced by Sharpening the SWIR Band.
  Remote Sens. 2016, 8, 354.
  '''

  # Read image as array
  S2_image_data=gdal.Open(S2_image).ReadAsArray().astype(np.float)

  # Estimate NDWI pixel values
  mndwi_10m=np.divide((S2_image_data[Dict_S2['B03'],:,:]-
S2_image_data[Dict_S2['B08'],:,:]),(S2_image_data[Dict_S2['B03'],:,:]+S2_i
mage_data[Dict_S2['B08'],:,:]))

  del S2_image_data

  return mndwi_10m
```

Function for Otsu thresholding for the NDWI and MNDWI indexes

```
def _compute_water_no_water_mask(S2_index):
  '''
  Using thresholding otsu approach create water- no_water mask
  '''

  # Calculate threshold using automatic otsu approach
  # Discard invalid pixels
  S2_index_1d = S2_index.flatten()
  S2_index_1d_values = S2_index_1d[np.nonzero(S2_index_1d)]
  thresh = threshold_otsu(S2_index_1d_values)
  water_mask = np.logical_and(S2_index > thresh, S2_index!=0)

  # Remove small objects
  water_mask_refined=morphology.remove_small_objects(water_mask.astype(np.
bool), 400)

  return water_mask_refined
```

Random Forest train and predict

```
# Create an np array of zeros with the shape of the image
water_labels_train = np.zeros(mndwi.shape).astype(np.bool)

# Set the water area for the training
water_labels_train[600:800, 300:500] = True

# Create an np array of zeros with the shape of the image
land_labels_train = np.zeros(mndwi.shape).astype(np.bool)

# Set the land area for the training
land_labels_train[200:400, :500] = True

n_samples = S2_image_numpy.shape[1] * S2_image_numpy.shape[2]
n_bands = S2_image_numpy.shape[0]
flat_pixels = S2_image_numpy.reshape((n_bands, n_samples)).T

# Set the train features for water and land
train_features_water = S2_image_numpy[:,water_labels_train].T
train_features_land = S2_image_numpy[:,land_labels_train].T
train_features = np.concatenate([train_features_w,train_features_l])
train_labels = np.zeros(train_features.shape[0])
train_labels[:train_features_water.shape[0]] = 1

# Instantiate model with 1000 decision trees
rf = RandomForestClassifier(n_jobs=-1,
n_estimators=100, class_weight='balanced')

# Train the model on training data
rf.fit(train_features, train_labels)

# Prediction
predictions_flat = rf.predict(flat_pixels)
predictions = predictions_flat.reshape(S2_image_numpy.shape[1],
S2_image_numpy.shape[2])
```

Comparison function

```
def Accuracy_metrics_calc(Ground_truth_gdal_raster, Lake_gdal_raster):

 # Load manual digitization rasters (ground truth)
 Ground_truth=gdal.Open(Ground_truth_gdal_raster).ReadAsArray()
  Ground_truth=Ground_truth>0

 # Load lake raster from automated method
 Lake=gdal.Open(Lake_gdal_raster).ReadAsArray()
 Lake_mask = ~np.isnan(Lake)

 Lake=Lake>0

 cf=confusion_matrix(Ground_truth.flatten(), Lake.flatten())

 # Accuracy is sum of diagonal divided by total observations
 accuracy = np.trace(cf) / float(np.sum(cf))
 precision = cf[1,1] / sum(cf[:,1]) # precision (i.e., user's accuracy)
 recall  = cf[1,1] / sum(cf[1,:]) # recall (i.e., producer's accuracy)
 f1_score = 2*precision*recall / (precision + recall)
 Kappa_score = cohen_kappa_score(Ground_truth.flatten(), Lake.flatten())
 accuracy_dict={'Overall_accuracy':accuracy,
                'Precision':precision,
                'Recall':recall,
                'F1_score':f1_score,
                'Kappa_score':Kappa_score}

 return accuracy_dict
```

Water level estimation functionalities

Loop to check in all ICESat-2 beams to get distinct dates that have measurements.

```
# Load all ICESat-2 file names
FILE_NAMES = glob.glob(mypath+'/*/*.h5')
df = pd.DataFrame(columns = ['date', 'lon', 'lat', 'segment_id','height'])
#df = gpd.GeoDataFrame(df, geometry=gpd.points_from_xy(df.lon, df.lat))

# Loop within all files
for n, FILE_NAME in enumerate(FILE_NAMES):

  with h5py.File(FILE_NAME, mode='r') as f:
    lats = []
    lons = []
    segment_ids = []
    heights = []

    # Collect measurements from all the beams
    for beam in ['1r', '2r', '3r', '1l', '2l', '3l']:
      latvar = f['/gt{}/segment_lat'.format(beam)]
      latitude = latvar[:]
      lats.extend(latitude)

      lonvar = f['/gt{}/segment_lon'.format(beam)]
      longitude = lonvar[:]
      lons.extend(longitude)

      dset_name = f['/gt{}/inland_water_body_id'.format(beam)]
      data = dset_name[:]
      segment_ids.extend(data)

      height_var = f['/gt{}/ht_ortho'.format(beam)] #segment_geoid
      height = height_var[:] #stdev_water_surf #water_depth
      heights.extend(height)

  df_ = pd.DataFrame(zip([FILE_NAME]*len(lons), lons, lats, segment_ids, heigh
ts),columns = ['date', 'lon', 'lat', 'segment_id', 'height'])
  df_ = df_[df_['segment_id'] == 14533]
  #df_ = gpd.GeoDataFrame(df_, geometry=gpd.points_from_xy(df_.lon, df_.lat))
  #df_ = df_.cx[21.2377:21.3613, 40.4599:40.5685]
  df = df.append(df_)

  #print (n, len(df_), len(df))

df
```

Department of Physical Geography and Ecosystem Science

Master Thesis in Geographical Information Science

1. *Anthony Lawther:* The application of GIS-based binary logistic regression for slope failure susceptibility mapping in the Western Grampian Mountains, Scotland (2008).
2. *Rickard Hansen:* Daily mobility in Grenoble Metropolitan Region, France. Applied GIS methods in time geographical research (2008).
3. *Emil Bayramov:* Environmental monitoring of bio-restoration activities using GIS and Remote Sensing (2009).
4. *Rafael Villarreal Pacheco:* Applications of Geographic Information Systems as an analytical and visualization tool for mass real estate valuation: a case study of Fontibon District, Bogota, Columbia (2009).
5. *Siri Oestreich Waage:* a case study of route solving for oversized transport: The use of GIS functionalities in transport of transformers, as part of maintaining a reliable power infrastructure (2010).
6. *Edgar Pimiento:* Shallow landslide susceptibility – Modelling and validation (2010).
7. *Martina Schäfer:* Near real-time mapping of floodwater mosquito breeding sites using aerial photographs (2010).
8. *August Pieter van Waarden-Nagel:* Land use evaluation to assess the outcome of the programme of rehabilitation measures for the river Rhine in the Netherlands (2010).
9. *Samira Muhammad:* Development and implementation of air quality data mart for Ontario, Canada: A case study of air quality in Ontario using OLAP tool. (2010).
10. *Fredros Oketch Okumu*: Using remotely sensed data to explore spatial and temporal relationships between photosynthetic productivity of vegetation and malaria transmission intensities in selected parts of Africa (2011).
11. *Svajunas Plunge:* Advanced decision support methods for solving diffuse water pollution problems (2011).
12. *Jonathan Higgins:* Monitoring urban growth in greater Lagos: A case study using GIS to monitor the urban growth of Lagos 1990 - 2008 and produce future growth prospects for the city (2011).
13. *Mårten Karlberg:* Mobile Map Client API: Design and Implementation for Android (2011).

14. *Jeanette McBride:* Mapping Chicago area urban tree canopy using color infrared imagery (2011).

15. *Andrew Farina:* Exploring the relationship between land surface temperature and vegetation abundance for urban heat island mitigation in Seville, Spain (2011).

16. *David Kanyari*: Nairobi City Journey Planner: An online and a Mobile Application (2011).

17. *Laura V. Drews:* Multi-criteria GIS analysis for siting of small wind power plants - A case study from Berlin (2012).

18. *Qaisar Nadeem:* Best living neighborhood in the city - A GIS based multi criteria evaluation of ArRiyadh City (2012).

19. *Ahmed Mohamed El Saeid Mustafa:* Development of a photo voltaic building rooftop integration analysis tool for GIS for Dokki District, Cairo, Egypt (2012).

20. *Daniel Patrick Taylor*: Eastern Oyster Aquaculture: Estuarine Remediation via Site Suitability and Spatially Explicit Carrying Capacity Modeling in Virginia's Chesapeake Bay (2013).

21. *Angeleta Oveta Wilson:* A Participatory GIS approach to *unearthing* Manchester's Cultural Heritage '*gold mine'* (2013).

22. *Ola Svensson:* Visibility and Tholos Tombs in the Messenian Landscape: A Comparative Case Study of the Pylian Hinterlands and the Soulima Valley (2013).

23. *Monika Ogden:* Land use impact on water quality in two river systems in South Africa (2013).

24. *Stefan Rova:* A GIS based approach assessing phosphorus load impact on Lake Flaten in Salem, Sweden (2013).

25. *Yann Buhot:* Analysis of the history of landscape changes over a period of 200 years. How can we predict past landscape pattern scenario and the impact on habitat diversity? (2013).

26. *Christina Fotiou:* Evaluating habitat suitability and spectral heterogeneity models to predict weed species presence (2014).

27. *Inese Linuza:* Accuracy Assessment in Glacier Change Analysis (2014).

28. *Agnieszka Griffin:* Domestic energy consumption and social living standards: a GIS analysis within the Greater London Authority area (2014).

29. *Brynja Guðmundsdóttir:* Detection of potential arable land with remote sensing and GIS - A Case Study for Kjósarhreppur (2014).

30. *Oleksandr Nekrasov:* Processing of MODIS Vegetation Indices for analysis of agricultural droughts in the southern Ukraine between the years 2000-2012 (2014).

31. *Sarah Tressel:* Recommendations for a polar Earth science portal in the context of Arctic Spatial Data Infrastructure (2014).

32. *Caroline Gevaert:* Combining Hyperspectral UAV and Multispectral Formosat-2 Imagery for Precision Agriculture Applications (2014).

33. *Salem Jamal-Uddeen:* Using GeoTools to implement the multi-criteria evaluation analysis - weighted linear combination model (2014).

34. *Samanah Seyedi-Shandiz:* Schematic representation of geographical railway network at the Swedish Transport Administration (2014).

35. *Kazi Masel Ullah:* Urban Land-use planning using Geographical Information System and analytical hierarchy process: case study Dhaka City (2014).

36. *Alexia Chang-Wailing Spitteler:* Development of a web application based on MCDA and GIS for the decision support of river and floodplain rehabilitation projects (2014).

37. *Alessandro De Martino:* Geographic accessibility analysis and evaluation of potential changes to the public transportation system in the City of Milan (2014).

38. *Alireza Mollasalehi:* GIS Based Modelling for Fuel Reduction Using Controlled Burn in Australia. Case Study: Logan City, QLD (2015).

39. *Negin A. Sanati:* Chronic Kidney Disease Mortality in Costa Rica; Geographical Distribution, Spatial Analysis and Non-traditional Risk Factors (2015).

40. *Karen McIntyre:* Benthic mapping of the Bluefields Bay fish sanctuary, Jamaica (2015).

41. *Kees van Duijvendijk:* Feasibility of a low-cost weather sensor network for agricultural purposes: A preliminary assessment (2015).

42. *Sebastian Andersson Hylander:* Evaluation of cultural ecosystem services using GIS (2015).

43. *Deborah Bowyer:* Measuring Urban Growth, Urban Form and Accessibility as Indicators of Urban Sprawl in Hamilton, New Zealand (2015).

44. *Stefan Arvidsson:* Relationship between tree species composition and phenology extracted from satellite data in Swedish forests (2015).

45. *Damián Giménez Cruz*: GIS-based optimal localisation of beekeeping in rural Kenya (2016).

46. *Alejandra Narváez Vallejo:* Can the introduction of the topographic indices in LPJ-GUESS improve the spatial representation of environmental variables? (2016).

47. *Anna Lundgren:* Development of a method for mapping the highest coastline in Sweden using breaklines extracted from high resolution digital elevation models (2016).

48. *Oluwatomi Esther Adejoro:* Does location also matter? A spatial analysis of social achievements of young South Australians (2016).

49. *Hristo Dobrev Tomov:* Automated temporal NDVI analysis over the Middle East for the period 1982 - 2010 (2016).

50. *Vincent Muller:* Impact of Security Context on Mobile Clinic Activities A GIS Multi Criteria Evaluation based on an MSF Humanitarian Mission in Cameroon (2016).

51. *Gezahagn Negash Seboka:* Spatial Assessment of NDVI as an Indicator of Desertification in Ethiopia using Remote Sensing and GIS (2016).

52. *Holly Buhler:* Evaluation of Interfacility Medical Transport Journey Times in Southeastern British Columbia. (2016).

53. *Lars Ole Grottenberg*: Assessing the ability to share spatial data between emergency management organisations in the High North (2016).

54. *Sean Grant:* The Right Tree in the Right Place: Using GIS to Maximize the Net Benefits from Urban Forests (2016).

55. *Irshad Jamal:* Multi-Criteria GIS Analysis for School Site Selection in Gorno-Badakhshan Autonomous Oblast, Tajikistan (2016).

56. *Fulgencio Sanmartín:* Wisdom-volkano: A novel tool based on open GIS and time-series visualization to analyse and share volcanic data (2016).

57. *Nezha Acil:* Remote sensing-based monitoring of snow cover dynamics and its influence on vegetation growth in the Middle Atlas Mountains (2016).

58. *Julia Hjalmarsson:* A Weighty Issue: Estimation of Fire Size with Geographically Weighted Logistic Regression (2016).

59. *Mathewos Tamiru Amato:* Using multi-criteria evaluation and GIS for chronic food and nutrition insecurity indicators analysis in Ethiopia (2016).

60. *Karim Alaa El Din Mohamed Soliman El Attar:* Bicycling Suitability in Downtown, Cairo, Egypt (2016).

61. *Gilbert Akol Echelai:* Asset Management: Integrating GIS as a Decision Support Tool in Meter Management in National Water and Sewerage Corporation (2016).

62. *Terje Slinning:* Analytic comparison of multibeam echo soundings (2016).

63. *Gréta Hlín Sveinsdóttir:* GIS-based MCDA for decision support: A framework for wind farm siting in Iceland (2017).

64. *Jonas Sjögren:* Consequences of a flood in Kristianstad, Sweden: A GIS-based analysis of impacts on important societal functions (2017).

65. *Nadine Raska:* 3D geologic subsurface modelling within the Mackenzie Plain, Northwest Territories, Canada (2017).

66. *Panagiotis Symeonidis*: Study of spatial and temporal variation of atmospheric optical parameters and their relation with PM 2.5 concentration over Europe using GIS technologies (2017).

67. *Michaela Bobeck:* A GIS-based Multi-Criteria Decision Analysis of Wind Farm Site Suitability in New South Wales, Australia, from a Sustainable Development Perspective (2017).

68. *Raghdaa Eissa*: Developing a GIS Model for the Assessment of Outdoor Recreational Facilities in New Cities Case Study: Tenth of Ramadan City, Egypt (2017).

69. *Zahra Khais Shahid*: Biofuel plantations and isoprene emissions in Svea and Götaland (2017).

70. *Mirza Amir Liaquat Baig*: Using geographical information systems in epidemiology: Mapping and analyzing occurrence of diarrhea in urban - residential area of Islamabad, Pakistan (2017).

71. *Joakim Jörwall*: Quantitative model of Present and Future well-being in the EU-28: A spatial Multi-Criteria Evaluation of socioeconomic and climatic comfort factors (2017).

72. *Elin Haettner*: Energy Poverty in the Dublin Region: Modelling Geographies of Risk (2017).

73. *Harry Eriksson*: Geochemistry of stream plants and its statistical relations to soil- and bedrock geology, slope directions and till geochemistry. A GIS-analysis of small catchments in northern Sweden (2017).

74. *Daniel Gardevärn:* PPGIS and Public meetings – An evaluation of public participation methods for urban planning (2017).

75. *Kim Friberg:* Sensitivity Analysis and Calibration of Multi Energy Balance Land Surface Model Parameters (2017).

76. *Viktor Svanerud:* Taking the bus to the park? A study of accessibility to green areas in Gothenburg through different modes of transport (2017).

77. *Lisa-Gaye Greene*: Deadly Designs: The Impact of Road Design on Road Crash Patterns along Jamaica's North Coast Highway (2017).

78. *Katarina Jemec Parker*: Spatial and temporal analysis of fecal indicator bacteria concentrations in beach water in San Diego, California (2017).

79. *Angela Kabiru*: An Exploratory Study of Middle Stone Age and Later Stone Age Site Locations in Kenya's Central Rift Valley Using Landscape Analysis: A GIS Approach (2017).

80. *Kristean Björkmann*: Subjective Well-Being and Environment: A GIS-Based Analysis (2018).

81. *Williams Erhunmonmen Ojo*: Measuring spatial accessibility to healthcare for people living with HIV-AIDS in southern Nigeria (2018).

82. *Daniel Assefa*: Developing Data Extraction and Dynamic Data Visualization (Styling) Modules for Web GIS Risk Assessment System (WGRAS). (2018).

83. *Adela Nistora*: Inundation scenarios in a changing climate: assessing potential impacts of sea-level rise on the coast of South-East England (2018).

84. *Marc Seliger*: Thirsty landscapes - Investigating growing irrigation water consumption and potential conservation measures within Utah's largest master-planned community: Daybreak (2018).

85. *Luka Jovičić*: Spatial Data Harmonisation in Regional Context in Accordance with INSPIRE Implementing Rules (2018).

86. *Christina Kourdounouli*: Analysis of Urban Ecosystem Condition Indicators for the Large Urban Zones and City Cores in EU (2018).

87. *Jeremy Azzopardi*: Effect of distance measures and feature representations on distance-based accessibility measures (2018).

88. *Patrick Kabatha*: An open source web GIS tool for analysis and visualization of elephant GPS telemetry data, alongside environmental and anthropogenic variables (2018).

89. *Richard Alphonce Giliba*: Effects of Climate Change on Potential Geographical Distribution of Prunus africana (African cherry) in the Eastern Arc Mountain Forests of Tanzania (2018).

90. *Eiður Kristinn Eiðsson*: Transformation and linking of authoritative multi-scale geodata for the Semantic Web: A case study of Swedish national building data sets (2018).

91. *Niamh Harty*: HOP!: a PGIS and citizen science approach to monitoring the condition of upland paths (2018).

92. *José Estuardo Jara Alvear*: Solar photovoltaic potential to complement hydropower in Ecuador: A GIS-based framework of analysis (2018).

93. *Brendan O'Neill*: Multicriteria Site Suitability for Algal Biofuel Production Facilities (2018).

94. *Roman Spataru*: Spatial-temporal GIS analysis in public health – a case study of polio disease (2018).

95. *Alicja Miodońska*: Assessing evolution of ice caps in Suðurland, Iceland, in years 1986 - 2014, using multispectral satellite imagery (2019).

96. *Dennis Lindell Schettini*: A Spatial Analysis of Homicide Crime's Distribution and Association with Deprivation in Stockholm Between 2010-2017 (2019).

97. *Damiano Vesentini*: The Po Delta Biosphere Reserve: Management challenges and priorities deriving from anthropogenic pressure and sea level rise (2019).

98. *Emilie Arnesten*: Impacts of future sea level rise and high water on roads, railways and environmental objects: a GIS analysis of the potential effects of increasing sea levels and highest projected high water in Scania, Sweden (2019).

99. *Syed Muhammad Amir Raza*: Comparison of geospatial support in RDF stores: Evaluation for ICOS Carbon Portal metadata (2019).

100. *Hemin Tofiq*: Investigating the accuracy of Digital Elevation Models from UAV images in areas with low contrast: A sandy beach as a case study (2019).

101. *Evangelos Vafeiadis*: Exploring the distribution of accessibility by public transport using spatial analysis. A case study for retail concentrations and public hospitals in Athens (2019).

102. *Milan Sekulic*: Multi-Criteria GIS modelling for optimal alignment of roadway by-passes in the Tlokweng Planning Area, Botswana (2019).

103. *Ingrid Piirisaar*: A multi-criteria GIS analysis for siting of utility-scale photovoltaic solar plants in county Kilkenny, Ireland (2019).

104. *Nigel Fox*: Plant phenology and climate change: possible effect on the onset of various wild plant species' first flowering day in the UK (2019).

105. *Gunnar Hesch*: Linking conflict events and cropland development in Afghanistan, 2001 to 2011, using MODIS land cover data and Uppsala Conflict Data Programme (2019).

106. *Elijah Njoku*: Analysis of spatial-temporal pattern of Land Surface Temperature (LST) due to NDVI and elevation in Ilorin, Nigeria (2019).

107. *Katalin Bunyevácz*: Development of a GIS methodology to evaluate informal urban green areas for inclusion in a community governance program (2019).

108. *Paul dos Santos*: Automating synthetic trip data generation for an agent-based simulation of urban mobility (2019).

109. *Robert O' Dwyer*: Land cover changes in Southern Sweden from the mid-Holocene to present day: Insights for ecosystem service assessments (2019).

110. *Daniel Klingmyr*: Global scale patterns and trends in tropospheric NO2 concentrations (2019).

111. *Marwa Farouk Elkabbany*: Sea Level Rise Vulnerability Assessment for Abu Dhabi, United Arab Emirates (2019).

112. *Jip Jan van Zoonen*: Aspects of Error Quantification and Evaluation in Digital Elevation Models for Glacier Surfaces (2020).

113. *Georgios Efthymiou*: The use of bicycles in a mid-sized city – benefits and obstacles identified using a questionnaire and GIS (2020).

114. *Haruna Olayiwola Jimoh*: Assessment of Urban Sprawl in MOWE/IBAFO Axis of Ogun State using GIS Capabilities (2020).

115. *Nikolaos Barmpas Zachariadis*: Development of an iOS, Augmented Reality for disaster management (2020).

116. *Ida Storm*: ICOS Atmospheric Stations: Spatial Characterization of CO2 Footprint Areas and Evaluating the Uncertainties of Modelled CO2 Concentrations (2020).

117. *Alon Zuta*: Evaluation of water stress mapping methods in vineyards using airborne thermal imaging (2020).

118. *Marcus Eriksson*: Evaluating structural landscape development in the municipality Upplands-Bro, using landscape metrics indices (2020).

119. *Ane Rahbek Vierø*: Connectivity for Cyclists? A Network Analysis of Copenhagen's Bike Lanes (2020).

120. *Cecilia Baggini*: Changes in habitat suitability for three declining Anatidae species in saltmarshes on the Mersey estuary, North-West England (2020).

121. *Bakrad Balabanian*: Transportation and Its Effect on Student Performance (2020).

122. *Ali Al Farid*: Knowledge and Data Driven Approaches for Hydrocarbon Microseepage Characterizations: An Application of Satellite Remote Sensing (2020).

123. *Bartlomiej Kolodziejczyk*: Distribution Modelling of Gene Drive-Modified Mosquitoes and Their Effects on Wild Populations (2020).

124. *Alexis Cazorla*: Decreasing organic nitrogen concentrations in European water bodies - links to organic carbon trends and land cover (2020).

125. *Kharid Mwakoba*: Remote sensing analysis of land cover/use conditions of community-based wildlife conservation areas in Tanzania (2021).

126. *Chinatsu Endo*: Remote Sensing Based Pre-Season Yellow Rust Early Warning in Oromia, Ethiopia (2021).

127. *Berit Mohr*: Using remote sensing and land abandonment as a proxy for long-term human out-migration. A Case Study: Al-Hassakeh Governorate, Syria (2021).

128. *Kanchana Nirmali Bandaranayake*: Considering future precipitation in delineation locations for water storage systems - Case study Sri Lanka (2021).

129. *Emma Bylund*: Dynamics of net primary production and food availability in the aftermath of the 2004 and 2007 desert locust outbreaks in Niger and Yemen (2021).

130. *Shawn Pace*: Urban infrastructure inundation risk from permanent sea-level rise scenarios in London (UK), Bangkok (Thailand) and Mumbai (India): A comparative analysis (2021).

131. *Oskar Evert Johansson*: The hydrodynamic impacts of Estuarine Oyster reefs, and the application of drone technology to this study (2021).

132. *Pritam Kumarsingh*: A Case Study to develop and test GIS/SDSS methods to assess the production capacity of a Cocoa Site in Trinidad and Tobago (2021).

133. *Muhammad Imran Khan*: Property Tax Mapping and Assessment using GIS (2021).

134. *Domna Kanari*: Mining geosocial data from Flickr to explore tourism patterns: The case study of Athens (2021).

135. *Mona Tykesson Klubien*: Livestock-MRSA in Danish pig farms (2021).

136. *Ove Njøten*: Comparing radar satellites. Use of Sentinel-1 leads to an increase in oil spill alerts in Norwegian waters (2021).

137. *Panagiotis Patrinos*: Change of heating fuel consumption patterns produced by the economic crisis in Greece (2021).

138. *Lukasz Langowski*: Assessing the suitability of using Sentinel-1A SAR multi-temporal imagery to detect fallow periods between rice crops (2021).

139. *Jonas Tillman*: Perception accuracy and user acceptance of legend designs for opacity data mapping in GIS (2022).

140. *Gabriela Olekszyk*: ALS (Airborne LIDAR) accuracy: Can potential low data quality of ground points be modelled/detected? Case study of 2016 LIDAR capture over Auckland, New Zealand (2022).

141. *Luke Aspland*: Weights of Evidence Predictive Modelling in Archaeology (2022).

142. *Luís Fareleira Gomes*: The influence of climate, population density, tree species and land cover on fire pattern in mainland Portugal (2022).

143. *Andreas Eriksson*: Mapping Fire Salamander (Salamandra salamandra) Habitat Suitability in Baden-Württemberg with Multi-Temporal Sentinel-1 and Sentinel-2 Imagery (2022).

144. *Lisbet Hougaard Baklid*: Geographical expansion rate of a brown bear population in Fennoscandia and the factors explaining the directional variations (2022).

145. *Victoria Persson*: Mussels in deep water with climate change: Spatial distribution of mussel (Mytilus galloprovincialis) growth offshore in the French Mediterranean with respect to climate change scenario RCP 8.5 Long Term and Integrated Multi-Trophic Aquaculture (IMTA) using Dynamic Energy Budget (DEB) modelling (2022).

146. *Benjamin Bernard Fabien Gérard Borgeais*: Implementing a multi-criteria GIS analysis and predictive modelling to locate Upper Palaeolithic decorated caves in the Périgord noir, France (2022).

147. *Bernat Dorado-Guerrero*: Assessing the impact of post-fire restoration interventions using spectral vegetation indices: A case study in El Bruc, Spain (2022).

148. *Ignatius Gabriel Aloysius Maria Perera*: The Influence of Natural Radon Occurrence on the Severity of the COVID-19 Pandemic in Germany: A Spatial Analysis (2022).

149. *Mark Overton*: An Analysis of Spatially-enabled Mobile Decision Support Systems in a Collaborative Decision-Making Environment (2022).

150. *Viggo Lunde*: Analysing methods for visualizing time-series datasets in open-source web mapping (2022).

151. *Johan Viscarra Hansson*: Distribution Analysis of Impatiens glandulifera in Kronoberg County and a Pest Risk Map for Alvesta Municipality (2022).

152. *Vincenzo Poppiti*: GIS and Tourism: Developing strategies for new touristic flows after the Covid-19 pandemic (2022).

153. *Henrik Hagelin*: Wildfire growth modelling in Sweden - A suitability assessment of available data (2023).

154. *Gabriel Romeo Ferriols Pavico*: Where there is road, there is fire (influence): An exploratory study on the influence of roads in the spatial patterns of Swedish wildfires of 2018 (2023).

155. *Colin Robert Potter*: Using a GIS to enable an economic, land use and energy output comparison between small wind powered turbines and large-scale wind farms: the case of Oslo, Norway (2023).

156. *Krystyna Muszel*: Impact of Sea Surface Temperature and Salinity on Phytoplankton blooms phenology in the North Sea (2023).

157. *Tobias Rydlinge*: Urban tree canopy mapping - an open source deep learning approach (2023).

158. *Albert Wellendorf*: Multi-scale Bark Beetle Predictions Using Machine Learning (2023).

159. *Manolis Papadakis*: Use of Satellite Remote Sensing for Detecting Archaeological Features: An Example from Ancient Corinth, Greece (2023).

160. *Konstantinos Sourlamtas*: Developing a Geographical Information System for a water and sewer network, for monitoring, identification and leak repair - Case study: Municipal Water Company of Naoussa, Greece (2023).

161. *Xiaoming Wang*: Identification of restoration hotspots in landscape-scale green infrastructure planning based on model-predicted connectivity forest (2023).

162. *Sarah Sienaert*: Usability of Sentinel-1 C-band VV and VH SAR data for the detection of flooded oil palm (2023).

163. *Katarina Ekeroot*: Uncovering the spatial relationships between Covid-19 vaccine coverage and local politics in Sweden (2023).

164. *Nikolaos Kouskoulis*: Exploring patterns in risk factors for bark beetle attack during outbreaks triggered by drought stress with harvester data on attacked trees: A case study in Southeastern Sweden (2023).

165. *Jonas Almén*: Geographic polarization and clustering of partisan voting: A local-level analysis of Stockholm Municipality (2023).

166. *Sara Sharon Jones*: Tree species impact on Forest Fire Spread Susceptibility in Sweden (2023).

167. *Takura Matswetu*: Towards a Geographic Information Systems and Data-Driven Integration Management. Studying holistic integration through spatial accessibility of services in Tampere, Finland. (2023).

168. *Duncan Jones*: Investigating the influence of the tidal regime on harbour porpoise *Phocoena phocoena* distribution in Mount's Bay, Cornwall (2023).

169. *Jason Craig Joubert*: A comparison of remote sensed semi-arid grassland vegetation anomalies detected using MODIS and Sentinel-3, with anomalies in ground-based eddy covariance flux measurements (2023).

170. *Anastasia Sarelli*: Land cover classification using machine-learning techniques applied to fused multi-modal satellite imagery and time series data (2024).

171. *Athanasios Senteles*: Integrating Local Knowledge into the Spatial Analysis of Wind Power: The case study of Northern Tzoumerka, Greece (2024).

172. *Rebecca Borg:* Using GIS and satellite data to assess access of green area for children living in growing cities (2024).

173. *Panagiotis–Dimitrios Tsachageas*: Multicriteria Evaluation in Real Estate Land-use Suitability Analysis: The case of Volos, Greece (2024).

174. *Hugo Nilsson*: Inferring lane-level topology of signalised intersections from aerial imagery and OpenStreetMap using deep learning (2024).

175. *Pavlos Alexantonakis*: Estimating lake water volume fluctuations using Sentinel-2 and ICESat-2 remote sensing data (2024).